OPEN ACCESS

Nonlinear State-Variable Method (NSVM) for Li-Ion Batteries: Finite-Element Method and Control Mode

JES Focus Issue on Mathematical Modeling of Electrochemical Systems at Multiple Scales in Honor of John Newman

Nonlinear State-Variable Method (NSVM) for Li-Ion Batteries: Finite-Element Method and Control Mode

Meng Guo,[a] Xinfang Jin,[b,*] and Ralph E. White[a,,z]**

[a]*Department of Chemical Engineering, University of South Carolina, Columbia, South Carolina 29208, USA*
[b]*Department of Mechanical Engineering, University of South Carolina, Columbia, South Carolina 29208, USA*

The finite element method (FEM) was used in our nonlinear state-variable method (NSVM) presented recently (*J. Electrochem. Soc.*, **164**, E3001 (2017)). The details of the application of the FEM to solve the lithium ion pseudo-2D (P2D) model equations using the NSVM are presented here for several control modes (constant current, voltage, power, or load). Validation of the method was performed by comparison to rigorous full-order models and experimental data. The FEM based NSVM shows excellent performance, and the estimated cell parameters are determined with a high confidence level.

Manuscript submitted March 29, 2017; revised manuscript received May 9, 2017. Published May 24, 2017. *This paper is part of the JES Focus Issue on Mathematical Modeling of Electrochemical Systems at Multiple Scales in Honor of John Newman.*

The pseudo-2D (P2D) model for Li-ion cells[1] has been widely applied. This model includes two spatial dimensions and several partial differential equations (PDE) which are coupled by nonlinear electrochemical kinetics.[2] The basic solution approach for the P2D model is to discretize the spatially-distributed PDE into a differential-algebraic equation (DAE) system. The finite difference method (FDM), finite volume method (FVM), and finite element method (FEM) have been used to discretize the P2D model.[3–11] For physics-based simulation of Li-ion batteries, the FEM is an excellent solution approach especially for complex multi-scale cell domains.[12–14] Although there are commercial finite element software packages (e.g., COMSOL Multiphysics) with the capability of solving the model equations, in-house code developed with scripting languages (i.e., MATLAB, FORTRAN, and Python) are still important due to their low cost and flexibility.

In our previous work,[15] we presented a nonlinear state variable modeling (NSVM) algorithm to reduce the computational cost for solving the P2D model over a high-frequency time domain. According to that NSVM work, the state variables in the diffusion equations are solved using the following approach:

$$\underline{\mathbf{x}}_k = \underline{\underline{\mathbf{\Lambda}}}\underline{\mathbf{x}}_{k-1} + \underline{\underline{\mathbf{\Lambda}'\mathbf{B}}}\underline{\mathbf{d}}_{k-1} \quad [1]$$

where $\underline{\mathbf{x}}_k$ and $\underline{\mathbf{x}}_{k-1}$ are vectors for the concentration states at current and previous time instances, $\underline{\mathbf{d}}_{k-1}$ is the source term vector at the previous time instance, and $\underline{\underline{\mathbf{\Lambda}}}$, $\underline{\underline{\mathbf{\Lambda}'}}$, and $\underline{\underline{\mathbf{B}}}$ are matrix operators. The source terms are solved by a nonlinear algebraic constraint:

$$\begin{bmatrix} \underline{\mathbf{d}}_k \\ y_k \end{bmatrix} = F\left(\underline{\mathbf{x}}_k, \underline{\mathbf{u}}_k\right) \quad [2]$$

where $\underline{\mathbf{u}}_k$ and y_k are respectively the inputs and outputs of the model. The above mentioned approach enables the P2D model to be solved under a high-frequency current signal with significant time efficiency (50+ times faster than a COMSOL baseline model). However, Reference 15 does not show the full details of the NSVM due to the limits on article length; in Equation 1, operators $\underline{\underline{\mathbf{\Lambda}}}$, $\underline{\underline{\mathbf{\Lambda}'}}$, and $\underline{\underline{\mathbf{B}}}$ come from a specific FEM formulation which was not presented in that article; in Equation 2, the detailed solution procedure is also based on the FEM formulation. Also, the published NSVM algorithm can only simulate current control and the results have not been compared with real data. Furthermore, some derivation steps involved in the FEM solution procedure can be applied potentially to develop a reduced-order-modeling (ROM) approach. Consequently, the following is presented in this article:

1) our procedure to implement the finite-element method for the P2D model equations;
2) extension of the NSVM to apply for voltage, power, and load control modes;
3) validation of the NSVM by comparison to experimental data.

Mathematical Model

As illustrated by Figure 1, the P2D model was developed based on a dual-foil representation for a Li-ion cell, in which the x dimension runs through the thicknesses of the domain layers (anode, separator, and cathode) and the r dimension represents the radius of the spherical active material particles. Several transport equations are defined, respectively, over the x and r dimensions and are coupled by the surface electrochemical reaction kinetics. These physics-based equations for the P2D model are listed in Table I. The solution approach for the solid particle diffusion equation (r dimension) was discussed previously.[15] Consequently, the following sections will focus on the equations in the x dimension.

Formulation of the governing equations.—Three partial differential equations (PDEs) in the x dimension in the electrode domains (diffusion and charge conservation in the electrolyte and charge conservation in the solid phase) are solved using the finite element method, and all the PDEs can be written in the following standard format:

$$\rho(x)\frac{\partial w}{\partial t} = \frac{\partial}{\partial x}\left[\mu(x,t)\frac{\partial w}{\partial x}\right] + \gamma(x)\, j_s(x,t) \quad [3]$$

where t is time, $w(x,t)$ is a field variable, $\rho(x)$ is the mass function, $\mu(x,t)$ is the transport coefficient, $\gamma(x)$ is the forcing function, and $j_s(x,t)$ is the current density for surface electrochemical reactions. The governing equation for the electrolyte charge conservation is given by:

$$\frac{\partial}{\partial x}\left(\kappa_L^{eff}\frac{\partial \phi_L}{\partial x}\right) - \frac{\partial}{\partial x}\left[\frac{2RT\kappa_L^{eff}}{Fc_L}\left(1-t^+\right)\frac{\partial c_L}{\partial x}\right] + a\, j_s = 0 \quad [4]$$

where ϕ_L is the electrical potential of the electrolyte, κ_L^{eff} is the effective electrical conductivity of the electrolyte, c_L is the concentration of the electrolyte, t^+ is the electrolyte transference number, a is the specific surface area of the solid phase, T is temperature, R is the universal gas constant, and F is the Faraday constant. To make Equation 4 consistent with the standard form, the diffusional current density term $\frac{2RT\kappa_L^{eff}}{Fc_L}(1-t^+)\frac{\partial c_L}{\partial x}$ is combined with the conductive current term

*Electrochemical Society Member.
**Electrochemical Society Fellow.
zE-mail: white@cec.sc.edu

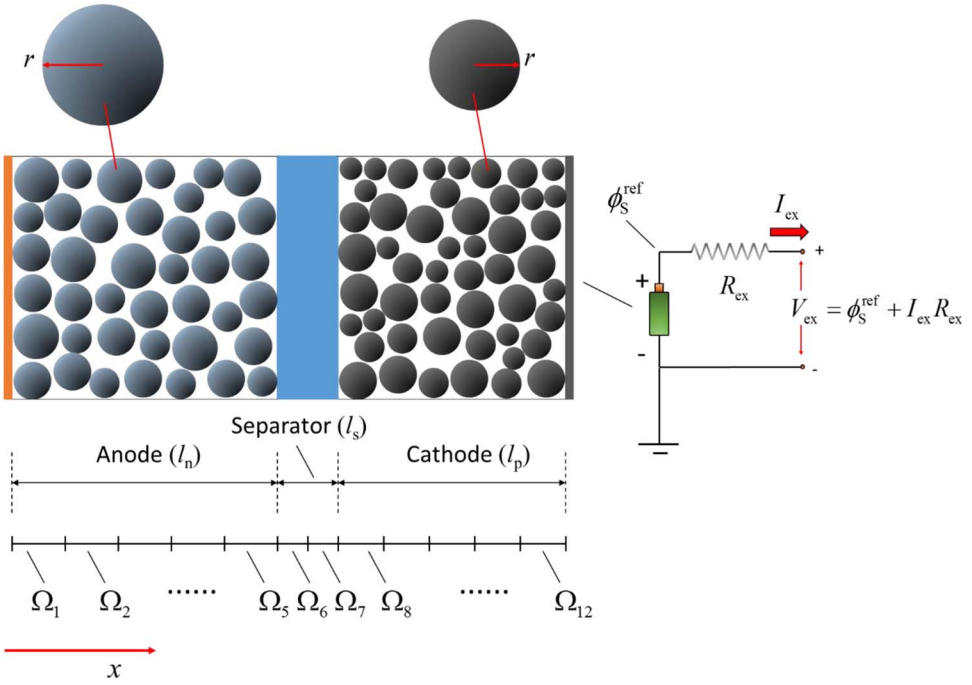

Figure 1. Schematic for pseudo-2D model: modeling domains, mesh pattern, and external electrical conditions.

$\kappa_L^{eff}\frac{\partial \phi_L}{\partial x}$ by introducing the modified electrolyte potential ϕ_L^*:

$$\phi_L^* = \phi_L - \frac{2RT}{F}\left(1 - t^+\right)\ln\left[\frac{c_L}{c_L\left(x = 0, t\right)}\right] - \phi_L^{ref} \quad [5]$$

where $\phi_L^{ref} = \phi_L|_{x=0}$ is the reference electrolyte potential selected for the boundary $x = 0$. Therefore, Equation 4 can be simplified to contain only one field variable ϕ_L^*:

$$\frac{\partial}{\partial x}\left(\kappa_L^{eff}\frac{\partial \phi_L^*}{\partial x}\right) + a j_s = 0 \quad [6]$$

and it can be derived from Equation 5 that $\phi_L^* = 0$ at boundary $x = 0$:

$$\phi_L^*\big|_{x=0} = 0 \quad [7]$$

where Equation 7 serves as the imposed boundary condition to determinate the absolute electrolyte potential values. The charge conservation in the solid phase is described by the following equation:

$$\frac{\partial}{\partial x}\left(\sigma_S^{eff}\frac{\partial \phi_S}{\partial x}\right) - a j_s = 0 \quad [8]$$

where ϕ_S is the potential of the solid phase and σ_S^{eff} is the effective electrical conductivity of the solid phase. As the solid phase potentials are distributed through two separate regions (anode and cathode), two imposed boundary conditions are set for both the anode at $x = 0$ and the cathode at $x = l_n + l_s + l_p$:

$$\phi_S|_{x=0} = 0 \quad \phi_S|_{x=l_n+l_s+l_p} = \phi_S^{ref} \quad [9]$$

Table I. Equations for pseudo-2D (P2D) model of Li-ion cell.

Physics	Equations
Electrolyte diffusion	$\varepsilon_L\frac{\partial c_L}{\partial t} = \frac{\partial}{\partial x}\left(D_L^{eff}\frac{\partial c_L}{\partial x}\right) + a(1-t^+)\frac{j_s}{F}$ $\frac{\partial c_L}{\partial x}\Big\|_{x=0} = 0$ $\frac{\partial c_L}{\partial x}\Big\|_{x=l_n+l_s+l_p} = 0$ $D_L^{eff} = D_{L,bulk}\varepsilon_L^{1.5}$ (Defined through $0 \le x \le l_n + l_s + l_p$ where $j_s = 0$ for $l_n \le x \le l_n + l_s$)
Electrolyte charge conservation	$\frac{\partial}{\partial x}\left(\kappa_L^{eff}\frac{\partial \phi_L}{\partial x}\right) - \frac{\partial}{\partial x}\left[\kappa_L^{eff}\frac{2RT}{F}\frac{(1-t^+)}{c_L}\frac{\partial c_L}{\partial x}\right] + a j_s = 0$ $\frac{\partial \phi_L}{\partial x}\Big\|_{x=0} = 0$ $\frac{\partial \phi_L}{\partial x}\Big\|_{x=l_n+l_s+l_p} = 0$ $\kappa_L^{eff} = \kappa_{L,bulk}\varepsilon_L^{1.5}$ (Defined through $0 \le x \le l_n + l_s + l_p$ where $j_s = 0$ for $l_n \le x \le l_n + l_s$)
Solid phase charge conservation	$\frac{\partial}{\partial x}\left(\sigma_S^{eff}\frac{\partial \phi_S}{\partial x}\right) - a j_s = 0$ $\sigma_S^{eff} = \sigma_S\varepsilon_S^{1.5}$ $-\sigma_S^{eff}\frac{\partial \phi_S}{\partial x}\Big\|_{x=0} = i_B(t)$ $\frac{\partial \phi_S}{\partial x}\Big\|_{x=l_n} = 0$ $\frac{\partial \phi_S}{\partial x}|_{x=l_n+l_s} = 0$ $-\sigma_S^{eff}\frac{\partial \phi_S}{\partial x}\Big\|_{x=l_n+l_s+l_p} = i_B(t)$ (Defined only for $0 \le x \le l_n$ and $l_n + l_s \le x \le l_n + l_s + l_p$)
Solid phase diffusion	$\frac{\partial c_S}{\partial t} = \frac{D_S}{r^2}\frac{\partial}{\partial r}\left(r^2\frac{\partial c_S}{\partial r}\right)$ $\frac{\partial c_S}{\partial r}\Big\|_{r=0} = 0$ $-D_S\frac{\partial c_S}{\partial r}\Big\|_{r=R_S} = \frac{j_s}{F}$ $\theta^* = \frac{c_S|_{r=R_S}}{c_{S,max}} = 0$ (Defined only for $0 \le x \le l_n$ and $l_n + l_s \le x \le l_n + l_s + l_p$)
Butler-Volmer equation	$\eta = \phi_S - \phi_L - j_s R_{film} - U$ $j_s = j_0(1-\theta^*)^{0.5}\theta^{*0.5}(\frac{c_L}{c_0})^{0.5}\left[\exp\left(\frac{0.5F}{RT}\eta\right) - \exp\left(-\frac{0.5F}{RT}\eta\right)\right]$ (Defined only for $0 \le x \le l_n$ and $l_n + l_s \le x \le l_n + l_s + l_p$), $R_{film} = 0$ for cathode
External conditions	$I_{ex} = -i_B(t)A_C$ $V_{ex} = \phi_S^{ref}(t) + I_{ex}R_{ex}$
Control equations	$I_{ex} = I_{app}(t)$(current control) $V_{ex} = V_{app}(t)$(voltage control) $I_{ex}V_{ex} = P_{app}(t)$(power control) $V_{ex} = -I_{ex}R_{load}(t)$(load control)

where ϕ_S^{ref} is the reference electrical potential of the cathode. Introduce the modified solid phase potential as follow:

$$\begin{aligned} \phi_S^* &= \phi_S \qquad \text{For anode domain } (0 \le x \le l_n) \\ \phi_S^* &= \phi_S - \phi_S^{ref} \qquad \text{For cathode domain } \left(l_n + l_s \le x \le l_n + l_s + l_p\right) \end{aligned} \quad [10]$$

The governing equation for ϕ_S^* is same as Equation 8,

$$\frac{\partial}{\partial x}\left(\sigma_S^{eff}\frac{\partial \phi_S^*}{\partial x}\right) - a j_s = 0 \quad [11]$$

and the imposed boundary conditions for ϕ_S^* are made homogeneous:

$$\phi_S^*\big|_{x=0} = 0 \quad \phi_S^*\big|_{x=l_n+l_s+l_p} = 0 \quad [12]$$

Accordingly, the overpotential of the electrodes can be expressed in terms of the modified potentials:

$$\begin{aligned} \eta &= \phi_S^* - \phi_L^* - U^* - j_s R_{film} - \phi_L^{ref} \qquad 0 \le x \le l_n \\ \eta &= \phi_S^* - \phi_L^* - U^* - \phi_L^{ref} + \phi_S^{ref} \qquad l_n + l_s \le x \le l_n + l_s + l_p \end{aligned} \quad [13]$$

where U^* denotes the modified open circuit potential expressed by

$$U^* = U\left(\theta^*\right) + \frac{2RT}{F}\left(1 - t^+\right)\ln\left[\frac{c_L}{c_L\left(x = 0, t\right)}\right] \quad [14]$$

Note that the SEI resistance R_{film} is neglected for the cathode and the definition of θ^* is given in Table I. With the introduction of ϕ_L^{ref} and ϕ_S^{ref}, two extra equations are needed to solve for these variables. Integration of Equation 8 through the two electrode domains yields the following equation:

$$\begin{aligned} &\int_0^{l_n} a j_s(x,t)\,dx + \int_{l_n+l_s}^{l_n+l_s+l_p} a j_s(x,t)\,dx \\ &= \sigma_S^{eff}\frac{\partial \phi_S}{\partial x}\bigg|_{x=0}^{x=l_n} + \sigma_S^{eff}\frac{\partial \phi_S}{\partial x}\bigg|_{x=l_n+l_s}^{x=l_n+l_s+l_p} \end{aligned} \quad [15]$$

The boundary current density for the solid phase is defined as follows:

$$\begin{aligned} -\sigma_S^{eff}\frac{\partial \phi_S}{\partial x}\bigg|_{x=0} &= i_B \quad \sigma_S^{eff}\frac{\partial \phi_S}{\partial x}\bigg|_{x=l_n} = 0 \quad \sigma_S^{eff}\frac{\partial \phi_S}{\partial x}\bigg|_{x=l_n+l_s} = 0 \\ -\sigma_S^{eff}\frac{\partial \phi_S}{\partial x}\bigg|_{x=l_n+l_s+l_p} &= i_B \end{aligned} \quad [16]$$

where i_B is the current density passing through the interfaces between the electrodes and the current collectors. Substituting boundary conditions 16 into the right-hand-side of Equation 15, the first limiting electrical equation is found to be:

$$\int_0^{l_n} a j_s(x,t)\,dx + \int_{l_n+l_s}^{l_n+l_s+l_p} a j_s(x,t)\,dx = 0 \quad [17]$$

Integration of Equation 8 through the cathode domain and application of the boundary conditions 16 yields the second limiting electrical equation as follows:

$$\int_0^{l_n} a j_s(x,t)\,dx = i_B \quad [18]$$

The diffusion of Li ions in the electrolyte phase is described by the following equation:

$$\varepsilon_L\frac{\partial c_L}{\partial t} = \frac{\partial}{\partial x}\left(D_L^{eff}\frac{\partial c_L}{\partial x}\right) + a\left(1 - t^+\right)\frac{j_s}{F} \quad [19]$$

where c_L is the concentration of electrolyte, ε_L is the volume fraction of electrolyte in the porous electrode, and D_L^{eff} is the effective diffusivity of the electrolyte in the porous electrode. As shown above, Equations 6, 11, and 19 are all consistent with the standard form given in Equation 3, and the interpretation for these equation variables are listed in Table II.

Table II. Expressions for variables in general Equation 3 according to different transport phenomena.

Symbol	Expression: Electrolyte diffusion	Expression: Electrolyte charge conservation	Expression: Solid phase charge conservation
$w(x,t)$	$c_L(x,t)$	$\phi_L^*(x,t)$	$\phi_S^*(x,t)$
$\rho(x)$	ε_L	0	0
$\mu(x,t)$	D_L^{eff}	κ_L^{eff}	σ_S^{eff}
$\gamma(x)$	$\frac{a(1-t^+)}{F}$	a	a

Mesh pattern for modeling domains.—The pseudo-2D model includes three computational domains: anode, separator, and cathode, and these domains are discretized into segmental elements ($\Omega_1, \Omega_2 \cdots$ shown in Figure 1). Let m_1, m_2, and m_3, respectively, denote the numbers of elements in the anode, separator, and cathode, so that Figure 1 presents a mesh pattern with $m_1 = 5$, $m_2 = 2$, and $m_3 = 5$. Three node points are defined, respectively, at the two ends and the center of each element. Figure 2 illustrates the indexing of nodes and elements, where the three nodes of the i^{th} element (Ω_i) are, respectively, labeled as x_{2i-1},x_{2i}, and x_{2i+1}, and node x_{2i+1} is shared by two adjacent elements Ω_i and Ω_{i+1} as the interior boundary. There are in total $2 \times (m_1 + m_2 + m_3) + 1$ nodes in the x dimension, where each domain contains $2m_{k=1,2,3} + 1$ nodes. Several integer parameters are specifically defined to facilitate our derivations:

$$\begin{aligned} m &= m_1 + m_2 + m_3 \\ m' &= m_1 + m_3 \\ n_1 &= 2m_1 + 1 \\ n_2 &= 2m_1 + 2m_2 + 1 \\ n' &= 2m_1 + 2m_3 + 2 \\ n &= 2m_1 + 2m_2 + 2m_3 + 1 \end{aligned} \quad [20]$$

where m denotes the total number of elements through the entire geometry, m' denotes the number of elements included in the two electrode domains where electrochemical reactions occur, n_1 is the node index for anode/separator interface, n_2 is the node index for separator/cathode interface, n' is the number of nodes included in the two electrode domains, and n is the total number of nodes through the entire geometry.

Basis functions.—Two types of basis functions are developed over the discretized geometry as shown in Figure 3. A series of piecewise quadratic polynomials $p_1(x)$, $p_2(x)$, $\cdots$, $p_n(x)$, whose expressions are given as below, are defined through node points:

$$p_1(x) = \begin{cases} \frac{(x-x_2)(x-x_3)}{(x_1-x_2)(x_1-x_3)} & \text{In element } \Omega_1 \\ 0 & \text{In other elements} \end{cases} \quad [21a]$$

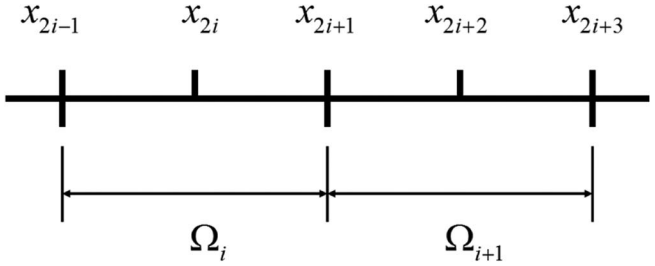

Figure 2. Illustration of mesh elements and nodes.

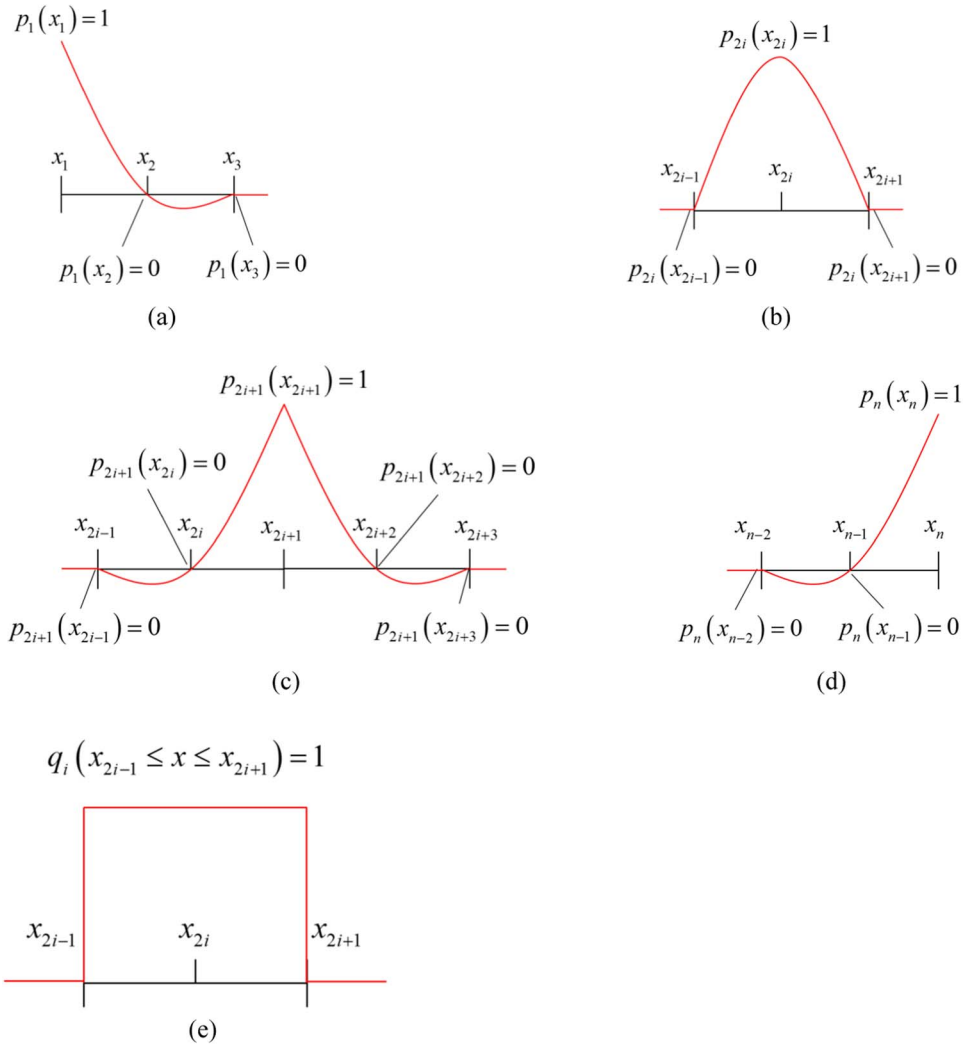

Figure 3. Definitions for node and element basis functions.

$$p_{2i}(x)=\begin{cases}\frac{(x-x_{2i-1})(x-x_{2i+1})}{(x_{2i}-x_{2i-1})(x_{2i}-x_{2i+1})} & \text{In element } \Omega_i\\ 0 & \text{In other elements}\end{cases}\quad i=1,2,\cdots,m \qquad [21b]$$

$$p_{2i+1}(x)=\begin{cases}\frac{(x-x_{2i})(x-x_{2i-1})}{(x_{2i+1}-x_{2i})(x_{2i+1}-x_{2i-1})} & \text{In element } \Omega_i\\ \frac{(x-x_{2i+2})(x-x_{2i+3})}{(x_{2i+1}-x_{2i+2})(x_{2i+1}-x_{2i+3})} & \text{In element } \Omega_{i+1}\\ 0 & \text{In other element}\end{cases}\quad i=1,2,\cdots,m-1 \qquad [21c]$$

$$p_n(x)=\begin{cases}\frac{(x-x_{n-1})(x-x_{n-2})}{(x_n-x_{n-1})(x_n-x_{n-2})} & \text{In element } \Omega_m\\ 0 & \text{In other elements}\end{cases} \qquad [21d]$$

The profiles for Equations 21a through 21d are respectively illustrated by Figures 3a, 3b, 3c, and 3d; it can be shown that the value of $p_i(x)$ at node point x_j $(i, j = 1, 2, \cdots, n)$ makes a Kronecker delta function:

$$p_i(x_j)=\begin{cases}1 & i=j\\ 0 & i\neq j\end{cases}\quad i,j=1,2,\cdots,n \qquad [22]$$

A series of boxcar functions $q_1(x), q_2(x), \cdots, q_m(x)$ are defined over the elements, whose expressions are given by:

$$q_i(x)=\begin{cases}1 & \text{In element } \Omega_i\\ 0 & \text{In other elements}\end{cases}\quad i=1,2,\cdots,m \qquad [23]$$

and Equation 23 is illustrated by Figure 3e.

Discretized variables.—Table III lists the variable vectors in the discretized P2D model. According to Equations (R-1) through (R-3), vectors $\underline{\mathbf{c}}_{\mathrm{L}}(t)$, $\underline{\mathbf{\Phi}}_{\mathrm{L}}(t)$, and $\underline{\mathbf{\Phi}}_{\mathrm{S}}(t)$ are made up by the nodal values of the field variables $c_{\mathrm{L}}(x,t)$, $\phi^*_{\mathrm{L}}(x,t)$, and $\phi^*_{\mathrm{S}}(x,t)$; the volume-average for these field variables in each element, $\hat{c}_{\mathrm{L},i}(t)$, $\hat{\phi}^*_{\mathrm{L},i}(t)$, and $\hat{\phi}^*_{\mathrm{S},i}(t)$, are defined by Equations (R-4) through (R-6), and vectors $\underline{\hat{\mathbf{c}}}_{\mathrm{L}}(t)$, $\underline{\hat{\mathbf{\Phi}}}_{\mathrm{L}}(t)$, and $\underline{\hat{\mathbf{\Phi}}}_{\mathrm{S}}(t)$ are formed by these element average values as shown in Equations (R-7) through(R-9). The electrochemical current density $j_{\mathrm{s}}(x,t)$ is assumed to be uniformly distributed in each element, and variables $j_{\mathrm{s},i}(t)$, which form vector $\underline{\mathbf{j}}_{\mathrm{s}}(t)$ as shown in Equation (R-10), stands for the homogenized element value for $j_{\mathrm{s}}(x,t)$. The vectors for basis functions are given by Equations (R-11) though (R-14), where vectors $\underline{\mathbf{p}}_{\mathrm{asc}}(x)$ and $\underline{\mathbf{q}}_{\mathrm{asc}}(x)$ are respectively formed by the node and element basis functions throughout the entire geometry(anode, separator, and cathode), and vectors $\underline{\mathbf{p}}_{\mathrm{ac}}(x)$ and $\underline{\mathbf{q}}_{\mathrm{ac}}(x)$ are respectively formed by the node and element basis functions in the two electrode domains. The effective electrolyte conductivity $\kappa^{\mathrm{eff}}_{\mathrm{L}}(x,t)$ is evaluated

Table III. Expressions for discretized variables.

Variable	Expression	Reference
$\underline{\mathbf{c}}_{\mathrm{L}}(t)$	$[c_{\mathrm{L}}(x_1,t), c_{\mathrm{L}}(x_2,t),\cdots, c_{\mathrm{L}}(x_n,t)]^{\tau}$	(R-1)
$\underline{\mathbf{\Phi}}_{\mathrm{L}}(t)$	$[\phi^*_{\mathrm{L}}(x_1,t), \phi^*_{\mathrm{L}}(x_2,t), \cdots, \phi^*_{\mathrm{L}}(x_n,t)]^{\tau}$	(R-2)
$\underline{\mathbf{\Phi}}_{\mathrm{S}}(t)$	$[\phi^*_{\mathrm{S}}(x_1,t), \phi^*_{\mathrm{S}}(x_2,t)\cdots, \phi^*_{\mathrm{S}}(x_{n_1},t), \phi^*_{\mathrm{S}}(x_{n_2},t), \phi^*_{\mathrm{S}}(x_{n_2+1},t), \cdots, \phi^*_{\mathrm{S}}(x_n,t)]^{\tau}$	(R-3)
$\hat{c}_{\mathrm{L},i}(t)$	$\frac{1}{x_{2i+1}-x_{2i-1}}\int_{x_{2i-1}}^{x_{2i+1}} c_{\mathrm{L}}(x,t)dx \quad i=1,2,\cdots,m$	(R-4)
$\hat{\phi}^*_{\mathrm{L},i}(t)$	$\frac{1}{x_{2i+1}-x_{2i-1}}\int_{x_{2i-1}}^{x_{2i+1}} \phi^*_{\mathrm{L}}(x,t)dx \quad \begin{array}{l} i=1,2,\cdots,m_1, m_1+m_2+1, \\ m_1+m_2+2,\cdots,m \end{array}$	(R-5)
$\hat{\phi}^*_{\mathrm{S},i}(t)$	$\frac{1}{x_{2i+1}-x_{2i-1}}\int_{x_{2i-1}}^{x_{2i+1}} \phi^*_{\mathrm{S}}(x,t)dx \quad \begin{array}{l} i=1,2,\cdots,m_1, m_1+m_2+1, \\ m_1+m_2+2,\cdots,m \end{array}$	(R-6)
$\underline{\hat{\mathbf{c}}}_{\mathrm{L}}(t)$	$[\hat{c}_{\mathrm{L},1}(t), \hat{c}_{\mathrm{L},2}(t), \cdots, \hat{c}_{\mathrm{L},n}(t)]^{\tau}$	(R-7)
$\underline{\hat{\mathbf{\Phi}}}_{\mathrm{L}}(t)$	$[\hat{\phi}^*_{\mathrm{L},1}(t), \hat{\phi}^*_{\mathrm{L},2}(t), \cdots, \hat{\phi}^*_{\mathrm{L},m_1}(t), \hat{\phi}^*_{\mathrm{L},m_1+m_2+1}(t), \hat{\phi}^*_{\mathrm{L},m_1+m_2+2}(t), \cdots, \hat{\phi}^*_{\mathrm{L},m}(t)]^{\tau}$	(R-8)
$\underline{\hat{\mathbf{\Phi}}}_{\mathrm{S}}(t)$	$[\hat{\phi}^*_{\mathrm{S},1}(t), \hat{\phi}^*_{\mathrm{S},2}(t), \cdots, \hat{\phi}^*_{\mathrm{S},m_1}(t), \hat{\phi}^*_{\mathrm{S},m_1+m_2+1}(t), \hat{\phi}^*_{\mathrm{S},m_1+m_2+2}(t), \cdots, \hat{\phi}^*_{\mathrm{S},m}(t)]^{\tau}$	(R-9)
$\underline{\mathbf{j}}_{\mathrm{s}}(t)$	$[j_{\mathrm{s},1}(t), j_{\mathrm{s},2}(t), \cdots, j_{\mathrm{s},m_1}(t), j_{\mathrm{s},m_1+m_2+1}(t), j_{\mathrm{s},m_1+m_2+2}(t), \cdots, j_{\mathrm{s},m}(t)]^{\tau}$	(R-10)
$\underline{\mathbf{p}}_{\mathrm{asc}}(x)$	$[p_1(x), p_2(x),\cdots, p_n(x)]^{\tau}$	(R-11)
$\underline{\mathbf{p}}_{\mathrm{ac}}(x)$	$[p_1(x), p_2(x)\cdots, p_{n_1}(x), p_{n_2}(x), p_{n_2+1}(x), \cdots, p_n(x)]^{\tau}$	(R-12)
$\underline{\mathbf{q}}_{\mathrm{asc}}(x)$	$[q_1(x), q_2(x), \cdots, q_m(x)]^{\tau}$	(R-13)
$\underline{\mathbf{q}}_{\mathrm{ac}}(x)$	$[q_1(x), q_2(x), \cdots, q_{m_1}(x), q_{m_1+m_2+1}(x), q_{m_1+m_2+2}(x), \cdots, q_m(x)]^{\tau}$	(R-14)
$\kappa^{\mathrm{eff}}_{\mathrm{L},i}$	$\kappa_{\mathrm{L,bulk}}[\hat{c}_{\mathrm{L},i}(t), T]\varepsilon_{\mathrm{L}}^{1.5} \; i=1,2,\cdots,m$	(R-15)
U^*_i	$U[\theta^*_i(t)] + \frac{2RT}{F}(1-t^+)\ln\left[\frac{\hat{c}_{\mathrm{L},i}(t)}{c_{\mathrm{L}}(x_1,t)}\right] \quad \begin{array}{l} i=1,2,\cdots,m_1, m_1+m_2+1, \\ m_1+m_2+2,\cdots,m \end{array}$	(R-16)
η_i	$\begin{array}{l} \hat{\phi}^*_{\mathrm{S},i}(t) - \hat{\phi}^*_{\mathrm{L},i}(t) - U^*_i - j_{\mathrm{s},i}R_{\mathrm{film}} - \phi^{\mathrm{ref}}_{\mathrm{L}}(t) \quad i=1,2,\cdots,m_1 \\ \hat{\phi}^*_{\mathrm{S},i}(t) - \hat{\phi}^*_{\mathrm{L},i}(t) - U^*_i - \phi^{\mathrm{ref}}_{\mathrm{L}}(t) + \phi^{\mathrm{ref}}_{\mathrm{S}}(t) \quad i=m_1+m_2+1, m_1+m_2+2,\cdots,m \end{array}$	(R-17)
$j_{\mathrm{ex},i}$	$j_0[1-\theta^*_i(t)]^{0.5}[\theta^*_i(t)]^{0.5}\left[\frac{\hat{c}_{\mathrm{L},i}(t)}{c_0}\right]^{0.5} \quad \begin{array}{l} i=1,2,\cdots,m_1, m_1+m_2+1, \\ m_1+m_2+2,\cdots,m \end{array}$	(R-18)
$\underline{\mathbf{U}}$	$[U^*_1, U^*_2, \cdots, U^*_{m_1}, U^*_{m_1+m_2+1}, U^*_{m_1+m_2+2}, \cdots, U^*_m]^{\tau}$	(R-19)
$\underline{\boldsymbol{\eta}}$	$[\eta_1, \eta_2, \cdots, \eta_{m_1}, \eta_{m_1+m_2+1}, \eta_{m_1+m_2+2}, \cdots, \eta_m(t)]^{\tau}$	(R-20)
$\underline{\underline{\mathbf{R}}}_{\mathrm{film}}$	$\begin{bmatrix} \underline{\underline{\mathbf{I}}}_{m_1\times m_1} & \underline{\underline{\mathbf{0}}}_{m_1\times m_3} \\ \underline{\underline{\mathbf{0}}}_{m_3\times m_1} & \underline{\underline{\mathbf{0}}}_{m_3\times m_3} \end{bmatrix} R_{\mathrm{film}}$ where $\underline{\underline{\mathbf{I}}}$ stands for identity matrix and $\underline{\underline{\mathbf{0}}}$ stands for all - zeroes matrix	(R-21)
$\underline{\underline{\mathbf{B}}}_{\mathrm{LS}}$	$\begin{bmatrix} -\underline{\mathbf{J}}_{m_1\times 1} & \underline{\mathbf{0}}_{m_1\times 1} \\ -\underline{\mathbf{J}}_{m_3\times 1} & \underline{\mathbf{J}}_{m_3\times 1} \end{bmatrix}$ where $\underline{\underline{\mathbf{J}}}$ stands for all - ones matrix	(R-22)
$Z_{\mathrm{k},i}$	$\frac{RT}{Fj_{\mathrm{ex},i}} \; i=1,2,\cdots,m_1, m_1+m_2+1, m_1+m_2+2,\cdots,m$	(R-23)
$\underline{\underline{\mathbf{Z}}}_{\mathrm{k}}$	$\mathrm{diag}(Z_{\mathrm{k},1}, Z_{\mathrm{k},2}, \cdots, Z_{\mathrm{k},m_1}, Z_{\mathrm{k},m_1+m_2+1}, Z_{\mathrm{k},m_1+m_2+2}, \cdots, Z_{\mathrm{k},m})$	(R-24)

using $\hat{c}_{\mathrm{L},i}(t)$ in each element according to Equation (R-15), where the expression for the bulk electrolyte conductivity $\kappa_{\mathrm{L,bulk}}(c_{\mathrm{L}}, T)$ is given in Appendix A; and $\kappa^{\mathrm{eff}}_{\mathrm{L}}(x,t)$ can be calculated by following expression:

$$\kappa^{\mathrm{eff}}_{\mathrm{L}}(x,t) = \sum_{i=1}^{m} q_i(x)\kappa^{\mathrm{eff}}_{\mathrm{L},i} \qquad [24]$$

where $\kappa^{\mathrm{eff}}_{\mathrm{L},i}$ is the effective electrolyte conductivity for element Ω_i as defined by (R-15). In each element, the solid phase diffusion can be regarded as a submodel in which $j_{\mathrm{s},i}(t)$ serves as the single input, and θ^*_i denotes the surface state-of-charge value corresponding to $j_{\mathrm{s},i}(t)$; the solution procedure for the solid phase diffusion is shown in Appendix B. Kinetic variables related to the electrochemical reactions are also homogenized in each element, in Equations (R-16) through (R-18), variables U^*_i, η_i, and $j_{\mathrm{ex},i}$ respectively denote the modified open circuit potential, the overpotential, and the exchange current density values in each element; and in Equations (R-19) and (R-20), variables U^*_i and η_i form vectors $\underline{\mathbf{U}}$ and $\underline{\boldsymbol{\eta}}$. With Equations (R-21) and (R-22), the overpotential vector $\underline{\boldsymbol{\eta}}$ can be expressed as follow:

$$\underline{\boldsymbol{\eta}} = \underline{\hat{\mathbf{\Phi}}}_{\mathrm{S}}(t) - \underline{\hat{\mathbf{\Phi}}}_{\mathrm{L}}(t) - \underline{\mathbf{U}} - \underline{\underline{\mathbf{R}}}_{\mathrm{film}}\underline{\mathbf{j}}_{\mathrm{s}}(t) + \underline{\underline{\mathbf{B}}}_{\mathrm{LS}}\begin{bmatrix} \phi^{\mathrm{ref}}_{\mathrm{L}}(t) \\ \phi^{\mathrm{ref}}_{\mathrm{S}}(t) \end{bmatrix} \qquad [25]$$

The Butler-Volmer equation in element Ω_i is given by:

$$j_{\mathrm{s},i} = j_{\mathrm{ex},i}\left[\exp\left(\frac{0.5F}{RT}\eta_i\right) - \exp\left(-\frac{0.5F}{RT}\eta_i\right)\right] \qquad [26]$$

where $i=1,2,\cdots,m_1,m_1+m_2+1,m_1+m_2+2,\cdots,m$. Take 1st order Taylor expansion for the right-hand-side of Equation 26:

$$\begin{aligned} &j_{\mathrm{ex},i}\left[\exp\left(\frac{0.5F}{RT}\eta_i\right) - \exp\left(-\frac{0.5F}{RT}\eta_i\right)\right] \\ &\approx j_{\mathrm{ex},i}\left[\left(1+\frac{0.5F}{RT}\eta_i\right) - \left(1-\frac{0.5F}{RT}\eta_i\right)\right] \end{aligned} \qquad [27]$$

and the following approximation can be derived from Equations 26 and 27:

$$\eta_i \approx Z_{\mathrm{k},i}j_{\mathrm{s},i}(t) \qquad [28]$$

where the expression for the kinetic resistance $Z_{\mathrm{k},i}$ is given by (R-23). Equation 28 can be expanded in matrix-vector format through a diagonal matrix $\underline{\underline{\mathbf{Z}}}_{\mathrm{k}}$ defined in Equation (R-24):

$$\underline{\boldsymbol{\eta}} \approx \underline{\underline{\mathbf{Z}}}_{\mathrm{k}}\underline{\mathbf{j}}_{\mathrm{s}}(t) \qquad [29]$$

Table IV. Definition of operators for different transport phenomena.

Operator	Expression		
	Electrolyte diffusion	Electrolyte charge conservation	Solid phase charge conservation
$\underline{\mathbf{w}}(t)$	$\underline{\mathbf{c}}_{\mathrm{L}}(t)$	$\underline{\mathbf{\Phi}}_{\mathrm{L}}(t)$	$\underline{\mathbf{\Phi}}_{\mathrm{S}}(t)$
$\underline{\mathbf{p}}(x)$	$\underline{\mathbf{p}}_{\mathrm{asc}}(x)$	$\underline{\mathbf{p}}_{\mathrm{ac}}(x)$	$\underline{\mathbf{p}}_{\mathrm{ac}}(x)$
$\underline{\hat{\mathbf{w}}}(t)$	$\underline{\hat{\mathbf{c}}}_{\mathrm{L}}(t)$	$\underline{\hat{\mathbf{\Phi}}}_{\mathrm{L}}(t)$	$\underline{\hat{\mathbf{\Phi}}}_{\mathrm{S}}(t)$
$\underline{\mathbf{q}}(x)$	$\underline{\mathbf{q}}_{\mathrm{asc}}(x)$	$\underline{\mathbf{q}}_{\mathrm{ac}}(x)$	$\underline{\mathbf{q}}_{\mathrm{ac}}(x)$
$\int_{\Sigma\Omega}\langle\rangle dx$	$\int_0^{l_{\mathrm{n}}+l_{\mathrm{s}}+l_{\mathrm{p}}}\langle\rangle dx$	$\int_0^{l_{\mathrm{n}}+l_{\mathrm{s}}+l_{\mathrm{p}}}\langle\rangle dx$	$\int_0^{l_{\mathrm{n}}}\langle\rangle dx+\int_{l_{\mathrm{n}}+l_{\mathrm{s}}}^{l_{\mathrm{n}}+l_{\mathrm{s}}+l_{\mathrm{p}}}\langle\rangle dx$
Bi	Empty set	Empty set	$\{1, n\}$
$\underline{\mathbf{L}}_{\mathrm{B}}$	$\underline{\mathbf{0}}_{n\times 1}$	$\underline{\mathbf{0}}_{n\times 1}$	$\underline{\mathbf{p}}(x_1)i_{\mathrm{B}}(t)-\underline{\mathbf{p}}(x_n)i_{\mathrm{B}}(t)$
$\underline{\mathbf{h}}$	N/A	$\underline{\mathbf{0}}_{n\times 1}$	$\underline{\mathbf{p}}(x_1)-\underline{\mathbf{p}}(x_n)$
$\underline{\underline{\mathbf{Br}}}$	N/A	$[\underline{\mathbf{p}}(x_1)]^{\tau}$	$[\underline{\mathbf{p}}(x_1), \underline{\mathbf{p}}(x_n)]^{\tau}$

Approximation for the dependent variables.—In Equation 3, the field variable $w(x,t)$ and source term $j_{\mathrm{s}}(x,t)$ are, respectively, approximated by

$$w(x,t)=\underline{\mathbf{p}}^{\tau}(x)\,\underline{\mathbf{w}}(t) \qquad [30]$$

$$j_{\mathrm{s}}(x,t)=\underline{\mathbf{q}}_{\mathrm{ac}}^{\tau}(x)\,\underline{\mathbf{j}}_{\mathrm{s}}(t) \qquad [31]$$

where expressions for the vectors $\underline{\mathbf{p}}(x)$ and $\underline{\mathbf{w}}(t)$ are given in Table IV. The element-average values for $w(x,t)$ are expressed by $\underline{\hat{\mathbf{w}}}(t)$ according to Table IV, and there exist a linear transform from $\underline{\mathbf{w}}(t)$ to $\underline{\hat{\mathbf{w}}}(t)$ given by:

$$\underline{\hat{\mathbf{w}}}(t)=\underline{\underline{\mathbf{H}}}\,\underline{\mathbf{w}}(t) \qquad [32]$$

in which the constant operator $\underline{\underline{\mathbf{H}}}$ is defined in Appendix C.

Weak form of the transport equations.—In this work, $\underline{\mathbf{p}}(x)$ is used as test function to derive the weak form; left multiply Equation 3 by the test function $\underline{\mathbf{p}}(x)$ and integrate through the domains to obtain,

$$\int_{\Sigma\Omega}\underline{\mathbf{p}}(x)\,\rho(x)\,\frac{\partial w}{\partial t}dx=\int_{\Sigma\Omega}\underline{\mathbf{p}}(x)\,\frac{\partial}{\partial x}\left[\mu(x,t)\,\frac{\partial w}{\partial x}\right]dx+\int_{\Sigma\Omega}\underline{\mathbf{p}}(x)\,\gamma(x)\,j_{\mathrm{s}}(x,t)\,dx \qquad [33]$$

where the definition for operator $\int_{\Sigma\Omega}\langle\rangle dx$ is given in Table IV. On the right hand side of Equation 33, the first term can be expanded using integration by parts:

$$\int_{\Sigma\Omega}\underline{\mathbf{p}}(x)\,\frac{\partial}{\partial x}\left[\mu(x,t)\,\frac{\partial w}{\partial x}\right]dx=\sum_{i\in Bi}\underline{\mathbf{p}}(x_i)\,n_{\mathrm{B}}\mu(x_i,t)\,\frac{\partial w}{\partial x}\bigg|_{x_i}-\int_{\Sigma\Omega}\frac{d\underline{\mathbf{p}}}{dx}\mu(x,t)\,\frac{\partial w}{\partial x}dx \qquad [34]$$

where n_{B} denotes the direction pointing out of the boundary, and Bi is the index set for the non-insulation boundary nodes (see Table IV).

Therefore Equation 33 can be written as follows:

$$\int_{\Sigma\Omega}\underline{\mathbf{p}}(x)\,\rho(x)\,\frac{\partial w}{\partial t}dx=\sum_{i\in Bi}\underline{\mathbf{p}}(x_i)\,n_{\mathrm{B}}\mu(x_i,t)\,\frac{\partial w}{\partial x}\bigg|_{x_i}-\int_{\Sigma\Omega}\frac{d\underline{\mathbf{p}}}{dx}\mu(x,t)\,\frac{\partial w}{\partial x}dx+\int_{\Sigma\Omega}\underline{\mathbf{p}}(x)\,\gamma(x)\,j_{\mathrm{s}}(x,t)\,dx \qquad [35]$$

Substitute $w(x,t)$ and $j_{\mathrm{s}}(x,t)$ with the approximate expressions shown in Equations 30 and 31, and Equation 35 can be written as follows:

$$\underline{\underline{\mathbf{M}}}\frac{d\underline{\mathbf{w}}}{dt}=-\underline{\underline{\mathbf{K}}}\underline{\mathbf{w}}(t)+\underline{\underline{\mathbf{F}}}\underline{\mathbf{j}}_{\mathrm{s}}(t)+\underline{\mathbf{L}}_{\mathrm{B}} \qquad [36]$$

where $\underline{\underline{\mathbf{M}}}$ is the mass matrix defined by

$$\underline{\underline{\mathbf{M}}}=\int_{\Sigma\Omega}\underline{\mathbf{p}}(x)\,\rho(x)\,\underline{\mathbf{p}}^{\tau}(x)dx \qquad [37]$$

$\underline{\underline{\mathbf{K}}}$ is the stiffness matrix defined by

$$\underline{\underline{\mathbf{K}}}=\int_{\Sigma\Omega}\frac{d\underline{\mathbf{p}}}{dx}\mu(x,t)\,\frac{d\underline{\mathbf{p}}^{\tau}}{dx}dx \qquad [38]$$

$\underline{\underline{\mathbf{F}}}$ is the forcing matrix defined by

$$\underline{\underline{\mathbf{F}}}=\int_{\Sigma\Omega}\underline{\mathbf{p}}(x)\,\gamma(x)\,\underline{\mathbf{q}}_{\mathrm{ac}}^{\tau}(x)\,dx \qquad [39]$$

and $\underline{\mathbf{L}}_{\mathrm{B}}$ is the boundary loading vector defined by

$$\underline{\mathbf{L}}_{\mathrm{B}}=\sum_{i\in Bi}\underline{\mathbf{p}}(x_i)\,n_{\mathrm{B}}\mu(x_i,t)\,\frac{\partial w}{\partial x}\bigg|_{x_i} \qquad [40]$$

Starting from the weak form Equation 36, we have presented in Ref. 15 the solution procedure for the electrolyte diffusion (in which $\underline{\mathbf{L}}_{\mathrm{B}}=\underline{\mathbf{0}}$ for the insulated boundaries) over a discrete time domain. In the following sections of this work, we will focus on solving the coupled charge conservation and electrochemical kinetics under different control modes.

Charge conservation equations.—For the charge conservation equations, the mass matrix $\underline{\underline{\mathbf{M}}}=\underline{\underline{\mathbf{0}}}$ and the boundary loading vector $\underline{\mathbf{L}}_{\mathrm{B}}$ can be expressed by $\underline{\mathbf{L}}_{\mathrm{B}}=\underline{\mathbf{h}}i_{\mathrm{B}}(t)$ as shown in Table IV; therefore, the weak form Equation 36 can be written as follows:

$$\underline{\underline{\mathbf{K}}}\underline{\mathbf{w}}(t)=\underline{\underline{\mathbf{F}}}\underline{\mathbf{j}}_{\mathrm{s}}(t)+\underline{\mathbf{h}}i_{\mathrm{B}}(t) \qquad [41]$$

The reference potential Equations 7 and 9 are expressed as:

$$\underline{\underline{\mathbf{Br}}}\underline{\mathbf{w}}(t)=\underline{\mathbf{0}} \qquad [42]$$

where the definition for the reference boundary operator $\underline{\underline{\mathbf{Br}}}$ is given in Table IV. The limiting electrical Equations 17 and 18 are, respectively, expressed as follows:

$$\underline{\mathbf{C}}_1\underline{\mathbf{j}}_{\mathrm{s}}(t)=0 \qquad [43]$$

$$\underline{\mathbf{C}}_2\underline{\mathbf{j}}_{\mathrm{s}}(t)=i_{\mathrm{B}}(t) \qquad [44]$$

and the operators $\underline{\mathbf{C}}_1$ and $\underline{\mathbf{C}}_2$ are given by:

$$\underline{\mathbf{C}}_1=\int_0^{l_{\mathrm{n}}}a\underline{\mathbf{q}}_{\mathrm{ac}}^{\tau}(x)\,dx+\int_{l_{\mathrm{n}}+l_{\mathrm{s}}}^{l_{\mathrm{n}}+l_{\mathrm{s}}+l_{\mathrm{p}}}a\underline{\mathbf{q}}_{\mathrm{ac}}^{\tau}(x)\,dx \qquad [45]$$

$$\underline{\mathbf{C}}_2=\int_0^{l_{\mathrm{n}}}a\underline{\mathbf{q}}_{\mathrm{ac}}^{\tau}(x)\,dx \qquad [46]$$

Left multiply Equation 42 by $\underline{\underline{\mathbf{Br}}}^{\tau}$ and add the result to Equation 39, then substitute $i_{\mathrm{B}}(t)$ with expression 44 to obtain,

$$\left(\underline{\underline{\mathbf{K}}}+\underline{\underline{\mathbf{Br}}}^{\tau}\underline{\underline{\mathbf{Br}}}\right)\underline{\mathbf{w}}(t)=\left(\underline{\underline{\mathbf{F}}}+\underline{\underline{\mathbf{hC}}}_2\right)\underline{\mathbf{j}}_{\mathrm{s}}(t) \quad [47]$$

and the expression for $\underline{\mathbf{w}}(t)$ can be written as follows:

$$\underline{\mathbf{w}}(t)=\left(\underline{\underline{\mathbf{K}}}+\underline{\underline{\mathbf{Br}}}^{\tau}\underline{\underline{\mathbf{Br}}}\right)^{-1}\left(\underline{\underline{\mathbf{F}}}+\underline{\underline{\mathbf{hC}}}_2\right)\underline{\mathbf{j}}_{\mathrm{s}}(t) \quad [48]$$

According to Equations 32 and 48, the element-average potentials can be expressed as follows:

$$\hat{\underline{\mathbf{w}}}(t)=\underline{\underline{\mathbf{Z}}}\underline{\mathbf{j}}_{\mathrm{s}}(t) \quad [49]$$

where the transport resistance operator is given by:

$$\underline{\underline{\mathbf{Z}}}=\underline{\underline{\mathbf{H}}}\left(\underline{\underline{\mathbf{K}}}+\underline{\underline{\mathbf{Br}}}^{\tau}\underline{\underline{\mathbf{Br}}}\right)^{-1}\left(\underline{\underline{\mathbf{F}}}+\underline{\underline{\mathbf{hC}}}_2\right) \quad [50]$$

Equation 49 can be written, respectively, for the electrolyte and solid phases:

$$\underline{\mathbf{\Phi}}_{\mathrm{L}}(t)=\underline{\underline{\mathbf{Z}}}_{\mathrm{L}}\underline{\mathbf{j}}_{\mathrm{s}}(t) \quad \underline{\mathbf{\Phi}}_{\mathrm{S}}(t)=\underline{\underline{\mathbf{Z}}}_{\mathrm{S}}\underline{\mathbf{j}}_{\mathrm{s}}(t) \quad [51]$$

Substitute expressions 51 into Equation 25, so that the overpotential can be written as a linear expression for $\underline{\mathbf{j}}_{\mathrm{s}}(t)$, $\phi_{\mathrm{L}}^{\mathrm{ref}}(t)$, and $\phi_{\mathrm{S}}^{\mathrm{ref}}(t)$:

$$\underline{\mathbf{\eta}}=\left(\underline{\underline{\mathbf{Z}}}_{\mathrm{S}}-\underline{\underline{\mathbf{Z}}}_{\mathrm{L}}-\underline{\underline{\mathbf{R}}}_{\mathrm{film}}\right)\underline{\mathbf{j}}_{\mathrm{s}}(t)-\underline{\mathbf{U}}+\underline{\underline{\mathbf{B}}}_{\mathrm{LS}}\begin{bmatrix}\phi_{\mathrm{L}}^{\mathrm{ref}}(t)\\ \phi_{\mathrm{S}}^{\mathrm{ref}}(t)\end{bmatrix} \quad [52]$$

Model linearization and approximate solution.—To solve the nonlinear Butler-Volmer equations with the Newton method, good initial guesses are important to reduce the numerical difficulties. Initial values can be determined from the linearized kinetics. Substitute the approximate expression 29 into Equation 52 to yield:

$$\underline{\underline{\mathbf{Z}}}_{\mathrm{k}}\tilde{\underline{\mathbf{j}}}_{\mathrm{s}}(t)=\left(\underline{\underline{\mathbf{Z}}}_{\mathrm{S}}-\underline{\underline{\mathbf{Z}}}_{\mathrm{L}}-\underline{\underline{\mathbf{R}}}_{\mathrm{film}}\right)\tilde{\underline{\mathbf{j}}}_{\mathrm{s}}(t)-\underline{\mathbf{U}}+\underline{\underline{\mathbf{B}}}_{\mathrm{LS}}\begin{bmatrix}\tilde{\phi}_{\mathrm{L}}^{\mathrm{ref}}(t)\\ \tilde{\phi}_{\mathrm{S}}^{\mathrm{ref}}(t)\end{bmatrix} \quad [53]$$

where $\tilde{\underline{\mathbf{j}}}_{\mathrm{s}}(t)$, $\tilde{\phi}_{\mathrm{L}}^{\mathrm{ref}}(t)$, and $\tilde{\phi}_{\mathrm{S}}^{\mathrm{ref}}(t)$ are approximate solutions for the corresponding variables. Vector $\tilde{\underline{\mathbf{j}}}_{\mathrm{s}}(t)$ can be determined from Equation 53 as follows:

$$\tilde{\underline{\mathbf{j}}}_{\mathrm{s}}(t)=\underline{\underline{\mathbf{Z}}}_{\Delta}^{-1}\underline{\underline{\mathbf{B}}}_{\mathrm{LS}}\begin{bmatrix}\tilde{\phi}_{\mathrm{L}}^{\mathrm{ref}}(t)\\ \tilde{\phi}_{\mathrm{S}}^{\mathrm{ref}}(t)\end{bmatrix}-\underline{\underline{\mathbf{Z}}}_{\Delta}^{-1}\underline{\mathbf{U}} \quad [54]$$

where the operator $\underline{\underline{\mathbf{Z}}}_{\Delta}$ is given by:

$$\underline{\underline{\mathbf{Z}}}_{\Delta}=\underline{\underline{\mathbf{Z}}}_{\mathrm{k}}-\underline{\underline{\mathbf{Z}}}_{\mathrm{S}}+\underline{\underline{\mathbf{Z}}}_{\mathrm{L}}+\underline{\underline{\mathbf{R}}}_{\mathrm{film}} \quad [55]$$

Substitute expression 54 into the limiting electrical Equations 43 and 44 to yield

$$\begin{bmatrix}\underline{\mathbf{C}}_1\\ \underline{\mathbf{C}}_2\end{bmatrix}\underline{\underline{\mathbf{Z}}}_{\Delta}^{-1}\underline{\underline{\mathbf{B}}}_{\mathrm{LS}}\begin{bmatrix}\tilde{\phi}_{\mathrm{L}}^{\mathrm{ref}}(t)\\ \tilde{\phi}_{\mathrm{S}}^{\mathrm{ref}}(t)\end{bmatrix}-\begin{bmatrix}\underline{\mathbf{C}}_1\\ \underline{\mathbf{C}}_2\end{bmatrix}\underline{\underline{\mathbf{Z}}}_{\Delta}^{-1}\underline{\mathbf{U}}=\begin{bmatrix}0\\ 1\end{bmatrix}i_{\mathrm{B}}(t) \quad [56]$$

and the reference potentials $\tilde{\phi}_{\mathrm{L}}^{\mathrm{ref}}(t)$, and $\tilde{\phi}_{\mathrm{S}}^{\mathrm{ref}}(t)$ can be expressed as linear functions of $i_{\mathrm{B}}(t)$:

$$\begin{bmatrix}\tilde{\phi}_{\mathrm{L}}^{\mathrm{ref}}(t)\\ \tilde{\phi}_{\mathrm{S}}^{\mathrm{ref}}(t)\end{bmatrix}=\left\{\begin{bmatrix}\underline{\mathbf{C}}_1\\ \underline{\mathbf{C}}_2\end{bmatrix}\underline{\underline{\mathbf{Z}}}_{\Delta}^{-1}\underline{\underline{\mathbf{B}}}_{\mathrm{LS}}\right\}^{-1}\begin{bmatrix}0\\ 1\end{bmatrix}i_{\mathrm{B}}(t)+\left\{\begin{bmatrix}\underline{\mathbf{C}}_1\\ \underline{\mathbf{C}}_2\end{bmatrix}\underline{\underline{\mathbf{Z}}}_{\Delta}^{-1}\underline{\underline{\mathbf{B}}}_{\mathrm{LS}}\right\}^{-1}\begin{bmatrix}\underline{\mathbf{C}}_1\\ \underline{\mathbf{C}}_2\end{bmatrix}\underline{\underline{\mathbf{Z}}}_{\Delta}^{-1}\underline{\mathbf{U}} \quad [57]$$

Left multiply Equation 57 by [0, 1] to yield the expression for $\tilde{\phi}_{\mathrm{S}}^{\mathrm{ref}}(t)$:

$$\tilde{\phi}_{\mathrm{S}}^{\mathrm{ref}}(t)=u_{\mathrm{B}}+z_{\mathrm{B}}i_{\mathrm{B}}(t) \quad [58]$$

where the coefficients u_{B} and z_{B} are given by:

$$u_{\mathrm{B}}=\begin{bmatrix}0&1\end{bmatrix}\left\{\begin{bmatrix}\underline{\mathbf{C}}_1\\ \underline{\mathbf{C}}_2\end{bmatrix}\underline{\underline{\mathbf{Z}}}_{\Delta}^{-1}\underline{\underline{\mathbf{B}}}_{\mathrm{LS}}\right\}^{-1}\begin{bmatrix}\underline{\mathbf{C}}_1\\ \underline{\mathbf{C}}_2\end{bmatrix}\underline{\underline{\mathbf{Z}}}_{\Delta}^{-1}\underline{\mathbf{U}}$$

$$z_{\mathrm{B}}=\begin{bmatrix}0&1\end{bmatrix}\left\{\begin{bmatrix}\underline{\mathbf{C}}_1\\ \underline{\mathbf{C}}_2\end{bmatrix}\underline{\underline{\mathbf{Z}}}_{\Delta}^{-1}\underline{\underline{\mathbf{B}}}_{\mathrm{LS}}\right\}^{-1}\begin{bmatrix}0\\ 1\end{bmatrix} \quad [59]$$

According to Equations 54 and 57, values for $\tilde{\underline{\mathbf{j}}}_{\mathrm{s}}(t)$, $\tilde{\phi}_{\mathrm{L}}^{\mathrm{ref}}(t)$, and $\tilde{\phi}_{\mathrm{S}}^{\mathrm{ref}}(t)$ can all be determined by setting $i_{\mathrm{B}}(t)$.

Electrical control equations.—For the current control mode, $i_{\mathrm{B}}(t)$ can be evaluated using the following equation:

$$i_{\mathrm{B}}(t)=-\frac{I_{\mathrm{app}}(t)}{A_{\mathrm{C}}} \quad [60]$$

where $I_{\mathrm{app}}(t)$ is the total current applied to the cell which is defined as positive in charge and negative in discharge, and A_{C} is the total area of the cathode/current collector interface. For voltage control mode, the control equation is given as follows:

$$V_{\mathrm{ex}}=V_{\mathrm{app}}(t) \quad [61]$$

where $V_{\mathrm{app}}(t)$ is the applied voltage and the terminal current I_{ex} and terminal voltage V_{ex} are defined as follows:

$$I_{\mathrm{ex}}=-i_{\mathrm{B}}(t)A_{\mathrm{C}} \quad [62]$$

$$V_{\mathrm{ex}}=\phi_{\mathrm{S}}^{\mathrm{ref}}(t)+I_{\mathrm{ex}}R_{\mathrm{ex}} \quad [63]$$

Substituting $\phi_{\mathrm{S}}^{\mathrm{ref}}(t)$ with expression 58 and according to Equations 62 and 63, the voltage control equation can be expressed as follow:

$$u_{\mathrm{B}}+z_{\mathrm{B}}i_{\mathrm{B}}(t)-i_{\mathrm{B}}(t)A_{\mathrm{C}}R_{\mathrm{ex}}=V_{\mathrm{app}}(t) \quad [64]$$

and $i_{\mathrm{B}}(t)$ can be solved from Equation 64 as follow:

$$i_{\mathrm{B}}(t)=-\frac{V_{\mathrm{app}}(t)-u_{\mathrm{B}}}{A_{\mathrm{C}}R_{\mathrm{ex}}-z_{\mathrm{B}}} \quad [65]$$

For the power control mode, the control equation is given as follows:

$$I_{\mathrm{ex}}V_{\mathrm{ex}}=P_{\mathrm{app}}(t) \quad [66]$$

where $P_{\mathrm{app}}(t)$ is the applied power. According to Equations 58, 62, and 63, the control Equation 66 can be expressed as follows:

$$-\left[u_{\mathrm{B}}+z_{\mathrm{B}}i_{\mathrm{B}}(t)-i_{\mathrm{B}}(t)A_{\mathrm{C}}R_{\mathrm{ex}}\right]i_{\mathrm{B}}(t)A_{\mathrm{C}}=P_{\mathrm{app}}(t) \quad [67]$$

and i_{B} can be determined from Equation 67 through the quadratic solution:

$$i_{\mathrm{B}}(t)=\frac{A_{\mathrm{C}}u_{\mathrm{B}}+\sqrt{(A_{\mathrm{C}}u_{\mathrm{B}})^2+4P_{\mathrm{app}}(t)A_{\mathrm{C}}(A_{\mathrm{C}}R_{\mathrm{ex}}-z_{\mathrm{B}})}}{2A_{\mathrm{C}}(A_{\mathrm{C}}R_{\mathrm{ex}}-z_{\mathrm{B}})} \quad [68]$$

Equation 68 contains a quadratic discriminant D_{m} which is determined as follows:

$$D_{\mathrm{m}}=(A_{\mathrm{C}}u_{\mathrm{B}})^2+4P_{\mathrm{app}}(t)A_{\mathrm{C}}(A_{\mathrm{C}}R_{\mathrm{ex}}-z_{\mathrm{B}}) \quad [69]$$

and the solution for i_{B} according to Equation 68 is valid only for $D_{\mathrm{m}}\geq 0$. Under high power conditions, the value for D_{m} might be negative, which means the linearized Butler-Volmer kinetics cannot guarantee a valid solution; in this case try the following equation:

$$i_{\mathrm{B}}(t)=\frac{u_{\mathrm{B}}}{2(A_{\mathrm{C}}R_{\mathrm{ex}}-z_{\mathrm{B}})} \quad [70]$$

For the load control mode, the correlation between terminal voltage V_{ex} and the load resistance $R_{\mathrm{load}}(t)$ is as follows:

$$V_{\mathrm{ex}}=-I_{\mathrm{ex}}R_{\mathrm{load}}(t) \quad [71]$$

According to Equations 62, 63, and 71, the expression for i_B in load control mode is as follows:

$$i_B(t) = \frac{u_B}{A_C[R_{ex} + R_{load}(t)] - z_B} \quad [72]$$

Note that the $i_B(t)$ values evaluated above are not accurate, they are only used to estimate the approximate solutions $\tilde{\underline{\mathbf{j}}}_s(t)$, $\tilde{\phi}_L^{ref}(t)$, and $\tilde{\phi}_S^{ref}(t)$, which are used as initial values for the nonlinear step.

Nonlinear refinement of solutions.—According to Equation 26, the residue for Butler-Volmer equation in element Ω_i is expressed as follows:

$$R_{BV,i} = j_{ex,i}\left[\exp\left(\frac{0.5F}{RT}\eta_i\right) - \exp\left(-\frac{0.5F}{RT}\eta_i\right)\right] - j_{s,i}(t) \quad [73]$$

where $R_{BV,i}$ is the Butler-Volmer equation residue and $i = 1, 2, \cdots, m_1, m_1+m_2+1, m_1+m_2+2, \cdots, m$. The residue vector for Butler-Volmer equations $\underline{\mathbf{R}}_{BV}$ are given by:

$$\underline{\mathbf{R}}_{BV} = \left[R_{BV,1}, R_{BV,2}, \cdots, R_{BV,m_1}, R_{BV,m_1+m_2+1}, R_{BV,m_1+m_2+2}, \cdots, R_{BV,m}\right]^\tau \quad [74]$$

According to Equations 43 and 44, the residues for the electrical limiting equations, $\underline{\mathbf{R}}_{LE}$, are given by:

$$\underline{\mathbf{R}}_{LE} = \begin{bmatrix}\underline{\mathbf{C}}_1 \\ \underline{\mathbf{C}}_2\end{bmatrix}\underline{\mathbf{j}}_s(t) - \begin{bmatrix}0 \\ 1\end{bmatrix} i_B(t) \quad [75]$$

For the current control mode, the residue for the control equation, $\underline{\mathbf{R}}_{CE}$, is given by:

$$\underline{\mathbf{R}}_{CE} = i_B(t) + \frac{I_{app}(t)}{A_C} \quad [76]$$

for voltage control mode, $\underline{\mathbf{R}}_{CE}$ given by:

$$\underline{\mathbf{R}}_{CE} = \phi_S^{ref}(t) - i_B(t) A_C R_{ex} - V_{app}(t) \quad [77]$$

and for power control mode, $\underline{\mathbf{R}}_{CE}$ is given by:

$$\underline{\mathbf{R}}_{CE} = \left[\phi_S^{ref}(t) - i_B(t) A_C R_{ex}\right] i_B(t) + \frac{P_{app}(t)}{A_C} \quad [78]$$

Define the unknown vector $\underline{\mathbf{y}}$ and the model residue vector $\underline{\mathbf{Res}}$ as follows:

$$\underline{\mathbf{y}} = \begin{bmatrix}\underline{\mathbf{j}}_s(t) \\ \phi_L^{ref}(t) \\ \phi_S^{ref}(t) \\ i_B(t)\end{bmatrix} \quad \underline{\mathbf{Res}} = \begin{bmatrix}\underline{\mathbf{R}}_{BV} \\ \underline{\mathbf{R}}_{LE} \\ \underline{\mathbf{R}}_{CE}\end{bmatrix} \quad [79]$$

The Jacobian matrix $\underline{\underline{\mathbf{Jac}}}$ is expressed as the derivative of $\underline{\mathbf{Res}}$ with respect to $\underline{\mathbf{y}}$:

$$\underline{\underline{\mathbf{Jac}}} = \frac{d\underline{\mathbf{Res}}}{d\underline{\mathbf{y}}} \quad [80]$$

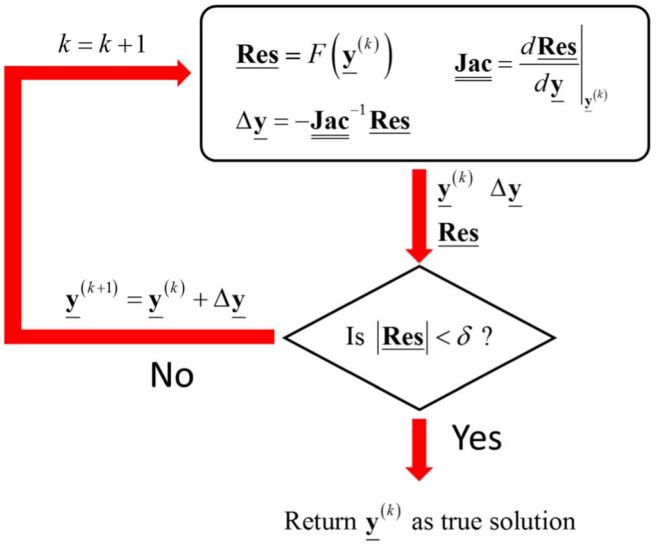

Figure 4. Newton loop for nonlinear solution.

and the step change for the unknown vector $\underline{\mathbf{y}}$ in each iteration can be calculated by:

$$\Delta\underline{\mathbf{y}} = -\underline{\underline{\mathbf{Jac}}}^{-1}\underline{\mathbf{Res}} \quad [81]$$

The solution for the nonlinear equations can be estimated with high accuracy using the Newton loop shown in Figure 4, where $\underline{\mathbf{y}}^{(k)}$ denotes the value of $\underline{\mathbf{y}}$ at the k^{th} iteration, and $\underline{\mathbf{y}}$ is updated with Equation 81 until the absolute value $|\underline{\mathbf{Res}}|$ is smaller than the tolerance δ (i.e., $\delta = 10^{-8}$).

Results and Discussion

In the previous work,[15] we have examined the accuracy of our NSVM algorithm for current control mode through model-to-model comparisons. In this work, we focus on model vs experimental validation and simulation of different control modes.

Model validation.—The computational algorithm described in Mathematical Model section was applied in modeling the Samsung commercial cells (the nominal cell capacity is 2.6 Ah), where the cell design parameters and basic physical properties are given in Appendix A. Three cells, labeled as LIB4, LIB6, and LIB7, respectively, were tested at room temperature ($T = 25^oC$) using different protocols. The experimental details for these cells are listed in Table V. MATLAB was used to develop the code for our cell model.

In simulation of the mixed cell control modes, the voltage control algorithm was applied for the constant voltage steps and the current control algorithm was applied for other steps. The cell temperature change was neglected in these simulations, and the SEI film resistance was only applied for the anode. Using the least-squares method,

Table V. Test protocols for different cells.

Cell	Test protocol	
	Charge	Discharge
LIB4	Charge at 1.25 C for 20 min — charge at 5/6 C for 18 min — charge at 0.5 C to 4.35 V — constant voltage at 4.35 V until current tapers to 0.05 CV — open circuit for 10 min	Discharge at 0.5 C for 60 min — discharge at 1 C for 15 min — discharge at 0.2 C until 2.75 V
LIB6	Charge at 0.7 C to 4.35 V — constant voltage at 4.35 V until current tapers to 0.05 V — open circuit for 10 min	Discharge at 0.2 C until 2.75 V
LIB7	Charge at 1 C to 4.35 V — constant voltage at 4.35 V until current tapers to 0.05 V — open circuit for 10 min	Discharge at 0.5 C for 60 min — discharge at 1 C for 15 min — discharge at 0.2 C until 2.75 V

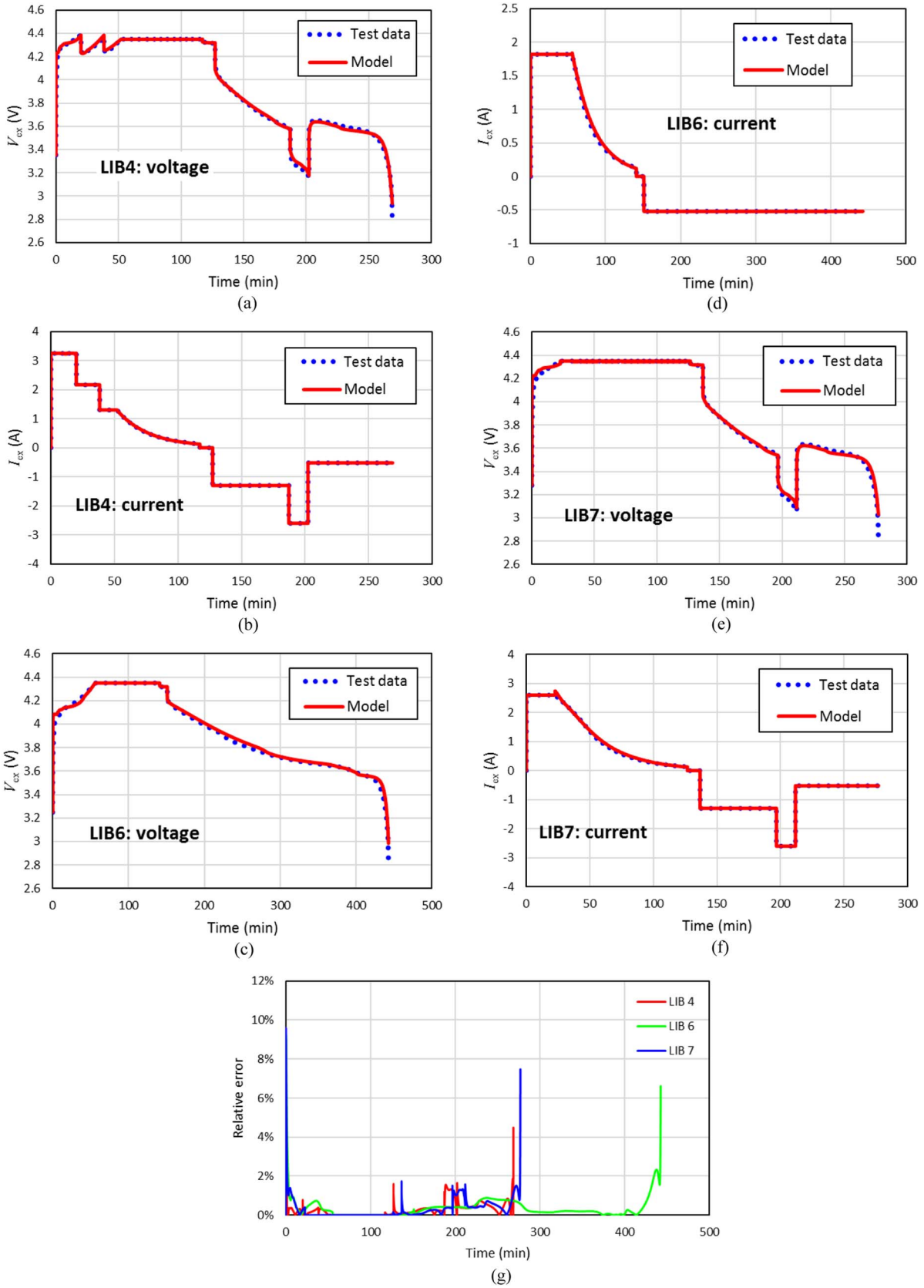

Figure 5. Optimized model predictions vs test data for cells: (a) voltage profiles for cell LIB4; (b) current profiles for cell LIB4; (c) voltage profiles for cell LIB6; (d) current profiles for cell LIB6; (e) voltage profiles for LIB7; (f) current profiles for cell LIB7; (g) Relative error plots for cell voltage between model and data.

Table VI. Estimated parameter values for different cells.

Parameter		Estimated values LIB4	LIB6	LIB7
SEI film resistance at anode R_{film} (Ωm^2)		0.1115	0.1413	0.1477
Solid phase diffusivity D_s (m^2/s)	Anode	1.3143×10^{-14}		
	Cathode	9.6117×10^{-14}		
Exchange current density j_0 (A/m^2)	Anode	29.867		
	Cathode	1.5986		

several cell parameters were estimated to fit the model to the test data. Among the estimated cell parameters, the solid phase diffusivities (D_s) and exchange current densities (j_{ex}) for the anode and cathode materials were assumed to be the same for all three cells, while the anode SEI film resistances varied between the cells. The optimized model results with comparisons to test data are presented in Figure 5 and the estimated parameter values are listed in Table VI. These results show that our NSVM algorithm works well with current and voltage control modes and the error for the model is below 2% for most parts of the simulated voltage profiles.

Power and load control simulation.—Using the optimized parameter sets from the previous section, our NSVM algorithm was implemented to simulate a power control step. The high frequency power input was scaled from the drive cycle current profile given in Ref. 15, where the applied power P_{app} is calculated as follow:

$$P_{app} = \text{C rate} \times I_{1C} \times 3\,[\text{V}] \qquad [82]$$

where $I_{1C} = 2.6$A is the 1 C rate current for the cell. The input profiles are shown in Figure 6, the power signal plot includes 8 periodic cycles and the peak power pulse of each cycle is around 17 W. The sampling frequency for the input power is 1 Hz or 1 data per second. The power control simulation was implemented for cell LIB4, and a rigorous model developed by COMSOL 5.2 was used as the baseline, in which the maximum time step is set to be 1 sec in accordance with the input sampling rate. The simulated voltage and current profiles are presented in Figure 7, and our algorithm shows excellent accuracy as compared with the baseline mode. However, it takes only 3.06 sec for our algorithm to finish the simulation as compared to the 762 sec for the baseline model. The simulated current profile in Figure 7a shows

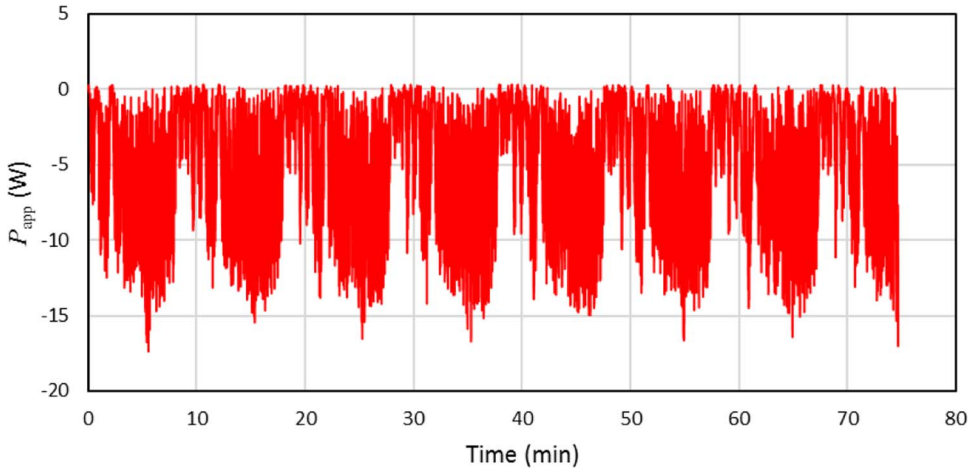

Figure 6. Input power profile obtained by scaling up the current values.

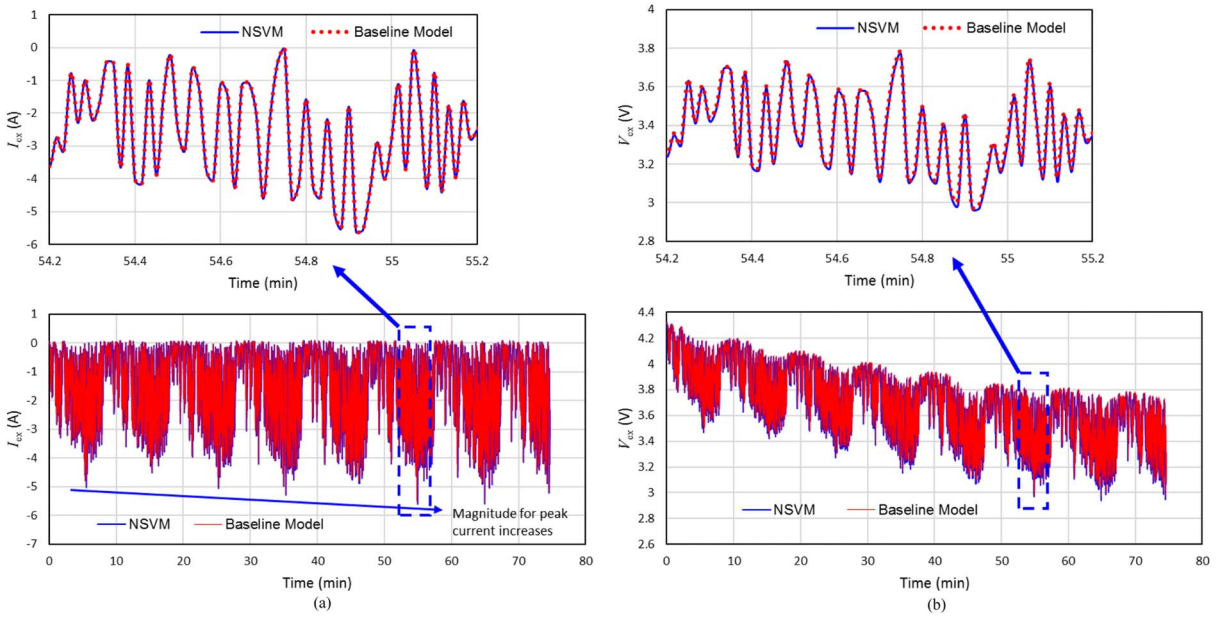

Figure 7. Results for power control simulation: (a) voltage profile; (b) current profile.

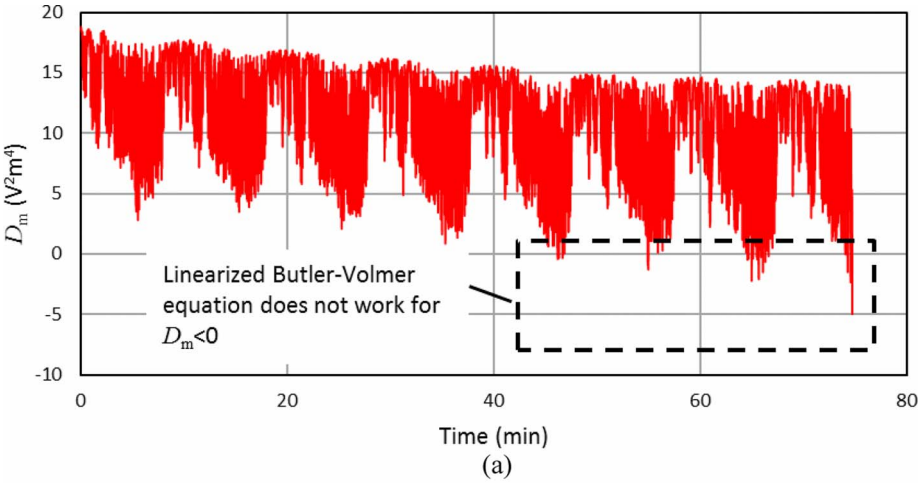

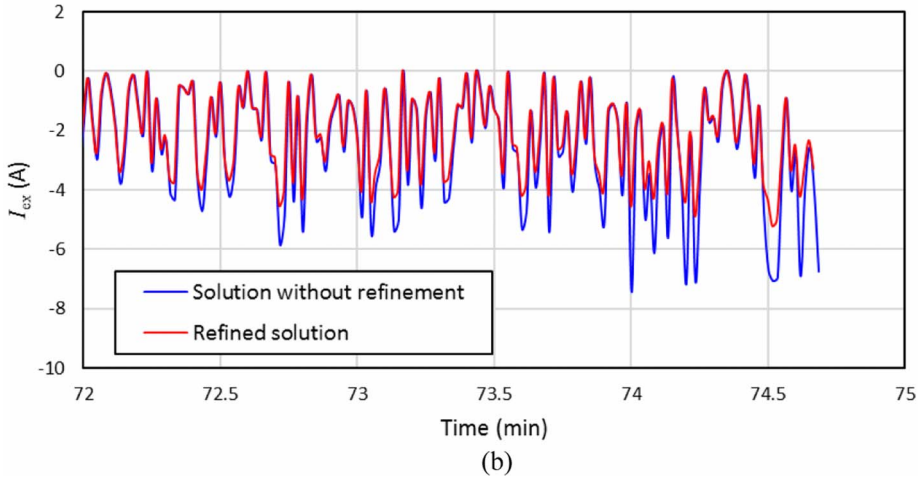

Figure 8. Results power control analysis: (a) plot for quadratic determinant; (b) current values calculated with/without nonlinear refinement.

that the magnitude for peak current in each cycle increases toward the end of discharge; the reason is that the power control mode requires $I_{ex}V_{ex} = P_{app}$, as the cell voltage V_{ex} drops with the depth of discharge, more current is needed to meet the power request. Other important results are presented in Figure 8 for analysis. The profile for the quadratic determinant D_m, which is defined in Equation 69, is plotted in Figure 8a and the results show that D_m takes negative values at high power pulses near the end of discharge; this suggests that a fully linearized model fails to provide valid solution at these points. In Figure 8b, the current values estimated by Equation 68 or Equation 70 are compared to those calculated through the nonlinear refinement loop (see Figure 4), the plots show that there are significant deviations between the two simulated current curves near the end of discharge, and these results suggest that the refinement loop is necessary to achieve good accuracy. To simulate the load control mode, a dynamic profile for the resistance load $R_{load}(t)$ was synthesized and presented in Figure 9. The simulated current and voltage profiles for the load control discharge are presented in Figures 10a and 10b. Similar to the power control results, the NSVM algorithm has excellent agreement with the baseline model, and the simulation takes only 3.24 sec for NSVM algorithm as contrast to the 510 sec for the baseline model. The error plots shown in Figure 11 confirm the accuracy of NSVM approach in the power and load control cases.

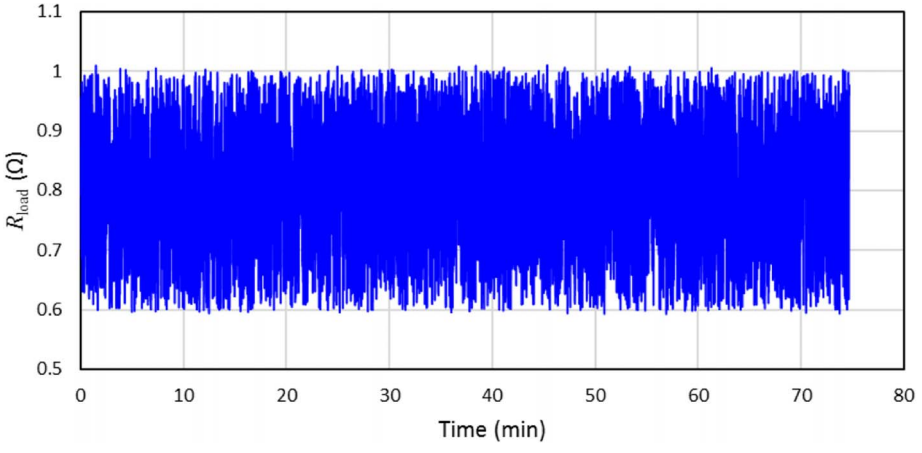

Figure 9. Synthesized profile for the load resistance.

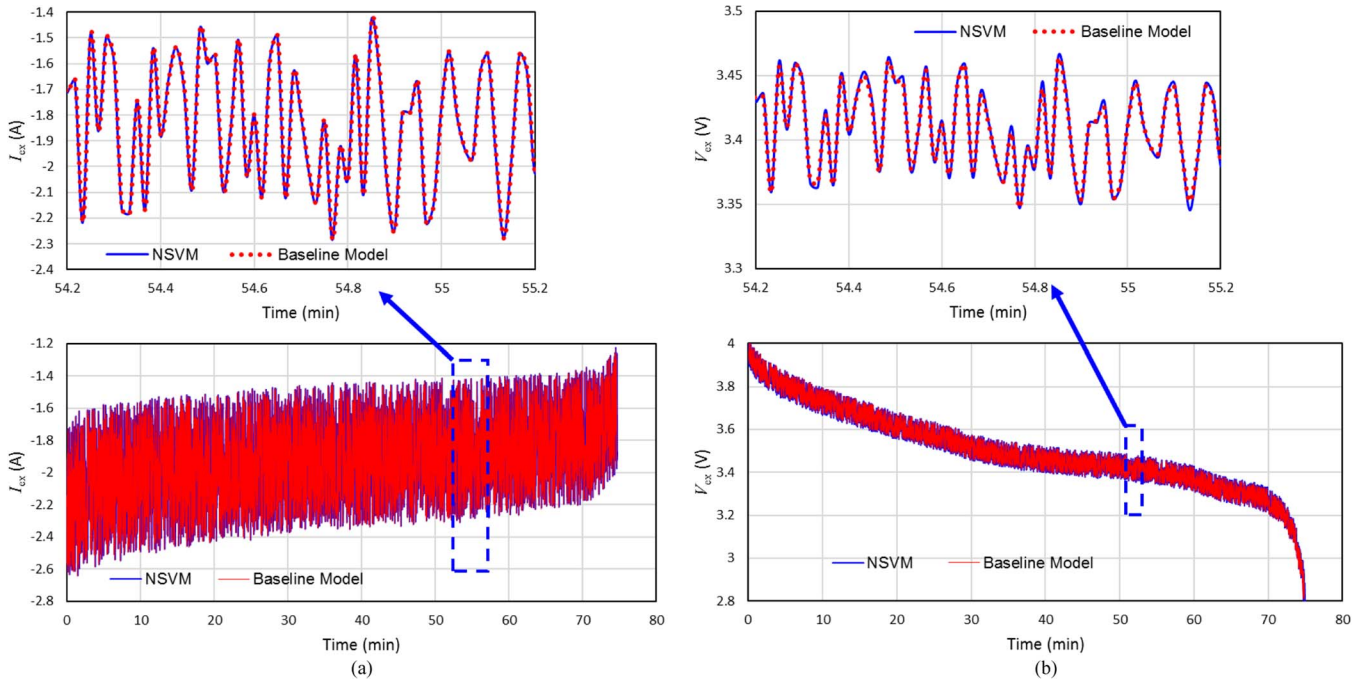

Figure 10. Results for load control simulation: (a) voltage profile; (b) current profile.

Numerical discussion.—As shown in Power and load control simulation section, the NSVM runs much faster than COMSOL and provides excellent accuracy. The time step approach presented by Equation 1 is the main reason for this significant improvement in simulation time efficiency. However, the FEM approach described in this article also contributes to this speedup. In COMSOL, the electrolyte and solid phase potentials ($\phi_L(x,t)$ and $\phi_S(x,t)$) are solved iteratively with the electrochemical current density ($j_s(x,t)$) at each node; in NSVM, only $j_s(x,t)$ is solved in the Newton loop and potential values are derived as linear expressions of $j_s(x,t)$. In addition, COMSOL defines the discretized current density $j_s(x,t)$ values at each node while NSVM defines $j_s(x,t)$ in each element, this means vector $\underset{\sim}{\mathbf{j}}_s(t)$ has smaller size in NSVM than in COMSOL. As $\underset{\sim}{\mathbf{j}}_s(t)$ is coupled with the solid phase diffusion, NSVM also includes fewer solid phase concentration variables than COMSOL. The FEM approach in NSVM greatly simplifies the solution procedure for the constraint Equation 2.

Conclusions

In this work, we made in-depth discussion on the application of finite element method to the P2D physic-based Li-ion cell model. Galerkin's weighted residual approach with quadratic basis functions was employed for our finite element analysis. The discretized field variables are defined into two categories: node variables and element variables, and the conversion between these two types of variables can be performed through a simple linear transform. The Butler-Volmer equations and the solid phase diffusion equations are solved in each element rather than at each node, which significantly lowers the computation load in simulation. We also developed simulation approaches for different battery control modes (current, voltage, load, and power control modes), and identified the limitations for a fully linearized model in the power control mode. For a linearized model, the Butler-Volmer equations are approximated using a 1st order Taylor series expansion, and the interface kinetic resistance is independent from the current density; when high power is applied, the linear polarization causes electrode potentials to drop sharply with increased current, and the cell might not meet the power request. Therefore, nonlinear compensation through are iterative Newton loop is important for the accuracy of model, because for nonlinear Butler-Volmer equations, the kinetic polarization drops exponentially with current density which prevents the cell voltage from being too low under high power. The model was also validated by test data with mixed current-voltage control modes and key parameters for the cell materials were estimated using least squares approach.

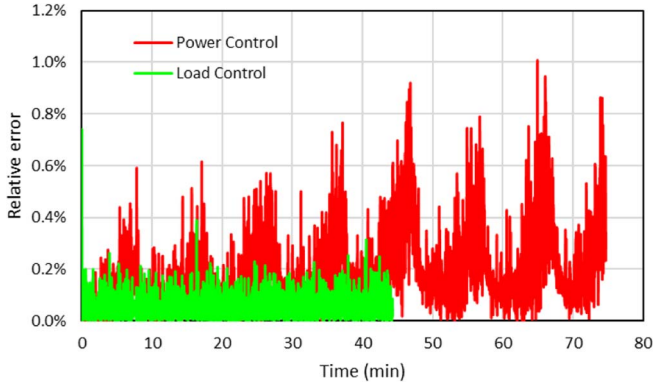

Figure 11. Relative error plots for cell voltage between NSVM and COMSOL.

Appendix A

The basic cell design parameters and physical properties are listed in Table A1. The electrical conductivity of bulk electrolyte is a function of electrolyte concentration and temperature:

$$\kappa_{L,bulk} = 3.45\exp\left(-\frac{798}{T}\right)\left(\frac{c_L}{1000}\right)^3 - 48.5\exp\left(-\frac{1080}{T}\right)\left(\frac{c_L}{1000}\right)^2 + 244\exp\left(-\frac{1440}{T}\right)\left(\frac{c_L}{1000}\right) \quad [A1]$$

The effective diffusivity and electrical conductivity for electrolyte is defined as follows:

$$D_L^{eff} = D_{L,bulk}\varepsilon_L^{1.5} \quad [A2]$$

$$\kappa_L^{eff} = \kappa_{L,bulk}\varepsilon_L^{1.5} \quad [A3]$$

Table A1. Design and physical parameters.

Parameter	Value		
	Anode	Separator	Cathode
Thickness l_n, l_s, l_p [m]	97.5×10^{-6}	17×10^{-6}	71×10^{-6}
Volume fraction of electrolyte ε_L	0.4	0.4	0.3
Volume fraction of active material ε_S	0.543		0.5978
Specific surface area of active material a [1/m]	1.8911×10^5		1.0625×10^5
Maximum Li concentration in active material c_{max} [mol/m^3]	30566		51555
Radius of active material particles R_s [m]	8.61×10^{-6}		16.88×10^{-6}
Electrical conductivity of solid phase σ_S [S/m]	100		3.8
Bulk electrolyte diffusivity at 25°C $D_{L,bulk}(T_{ref})$ [m^2/s]		5.6937×10^{-11}	
Transference number of electrolyte t^+		0.363	
Area of the cathode/current collector interface A_C [m^2]		0.0658	
External ohmic resistance R_{ex} [Ω]		0.0152	
Average electrolyte concentration c_0 [mol/m^3]		1200	
Universal gas constant R [J/mol/K]		8.3143	
Faraday constant F [C/mol]		96485	
Reference temperature T_{ref} [°C]		25	

and the effective electrical conductivity of solid phase is defined as follow:

$$\sigma_S^{eff} = \sigma_S \varepsilon_S^{1.5} \quad [A4]$$

The open circuit potentials for anode and cathode materials (U) are functions of the surface state-of-charge of solid phase (θ^*), and the U vs θ^* profiles are presented in Figure A1.

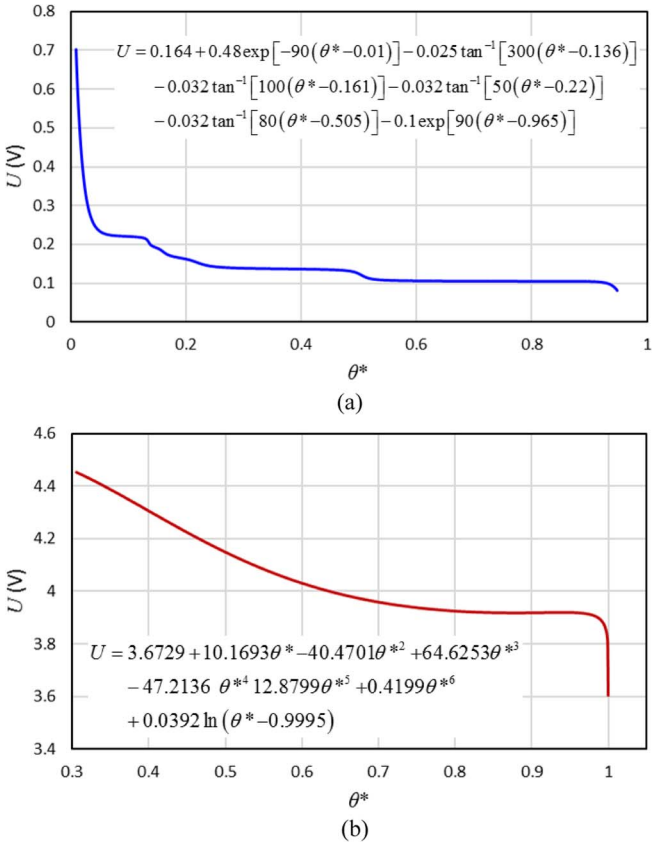

Figure A1. Open circuit potential profiles for active materials: (a) anode material; (b) cathode material.

Appendix B

The surface state-of-charge for solid phase, $\theta_i^*(t)$, is calculated as follows:

$$\theta_i^* = \theta_{avg,i} + \sum_{k=1}^{4} Q_{i,k}(t)$$
$$i = 1, 2, \cdots, m_1, m_1 + m_2 + 1, m_1 + m_2 + 2, \cdots, m \quad [B1]$$

where $\theta_{avg,i}(t)$ is the particle-average state-of-charge for the solid phase, and $Q_{i,k}(t)$ ($k = 1, 2, 3, 4$) are eigenfunctions. The governing equation for $\theta_{avg,i}(t)$ is as follows:

$$\frac{d\theta_{avg,i}}{dt} = -\frac{3 j_{s,i}(t)}{F R_s c_{max}}$$
$$i = 1, 2, \cdots, m_1, m_1 + m_2 + 1, m_1 + m_2 + 2, \cdots, m \quad [B2]$$

where c_{max} is the maximum concentration of the solid phase, and R_s is the radius of the solid phase particles. The governing equation for $Q_i(x, t)$ ($i = 1, 2, 3, 4$) is as follows:

$$\frac{\partial Q_{i,k}}{\partial t} = -\frac{a_k D_s}{R_s^2} Q_{i,k}(t) + \frac{b_k j_{s,i}(t)}{F R_s c_{max}} k = 1, 2, 3, 4$$
$$i = 1, 2, \cdots, m_1, m_1 + m_2 + 1, m_1 + m_2 + 2, \cdots, m \quad [B3]$$

where D_s is the solid phase diffusivity, and values for coefficients a_k and b_k ($k = 1, 2, 3, 4$) are listed in Table B1. The details for the derivation of these equations are provided in Ref. 15. As shown above, the dependent variables for the solid phase diffusion are associated with the surface electrochemical current density $j_s(x, t)$ in each element, and therefore are defined as element variables.

Appendix C

According to the definition in Equation 23, the following rule can be derived for element basis function $q_i(x)$:

$$q_i(x) q_j(x) = \begin{cases} q_i(x) & i = j \\ 0 & i \neq j \end{cases} \quad i, j = 1, 2, \cdots, m \quad [C1]$$

therefore the product for $\underline{\mathbf{q}}(x)\underline{\mathbf{q}}^{\tau}(x)$ yields a diagonal matrix as follow:

$$\underline{\mathbf{q}}(x)\,\underline{\mathbf{q}}^{\tau}(x) = \mathrm{diag}\,[q_1(x), q_2(x), \cdots, q_m(x)] \quad [C2]$$

The integral of $q_i(x)$ over the cell geometry equals to the length of element Ω_i:

$$\int_{\Sigma\Omega} q_i(x)\,dx = x_{2i+1} - x_{2i-1} = \Delta x_i \quad [C3]$$

Table B1. Values for coefficients in Equation B3.

	$k = 1$	$k = 2$	$k = 3$	$k = 4$
a_k	35058.7	1382.966	141.595	22.32279
b_k	−268.261	−30.9242	−7.59606	−2.59525

therefore the integrals for matrix $\underline{\mathbf{q}}(x)\underline{\mathbf{q}}^{\tau}(x)$ can be expressed as follows:

$$\int_{\Sigma\Omega} \underline{\mathbf{q}}(x)\,\underline{\mathbf{q}}^{\tau}(x)\,dx = \mathrm{diag}\,(\Delta x_1, \Delta x_2, \cdots, \Delta x_m) \qquad [C4]$$

The integral of $q_i(x)w(x,t)$ over the cell geometry equals to the integral $w(x,t)$ of over element Ω_i:

$$\int_{\Sigma\Omega} q_i(x)\,w(x,t)\,dx = \int_{x_{2i-1}}^{x_{2i+1}} w(x,t)\,dx \qquad [C5]$$

therefore the integral of vector $\underline{\mathbf{q}}(x)w(x,t)$ is expressed as follow:

$$\int_{\Sigma\Omega} \underline{\mathbf{q}}(x)\,w(x,t)\,dx = \left[\int_{x_1}^{x_3} w(x,t)\,dx, \int_{x_3}^{x_5} w(x,t)\,dx, \cdots, \int_{x_{2m-1}}^{x_{2m+1}} w(x,t)\,dx\right]^{\tau} \qquad [C6]$$

and the element-average vector $\underline{\hat{\mathbf{w}}}(t)$ can be calculated as follow:

$$\underline{\hat{\mathbf{w}}}(t) = \left[\int_{\Sigma\Omega} \underline{\mathbf{q}}(x)\,\underline{\mathbf{q}}^{\tau}(x)\,dx\right]^{-1} \int_{\Sigma\Omega} \underline{\mathbf{q}}(x)\,w(x,t)\,dx \qquad [C7]$$

Substitute $w(x,t) \approx \underline{\mathbf{p}}^{\tau}(x)\underline{\mathbf{w}}(t)$ into Equation C7 to yield

$$\left\{\left[\int_{\Sigma\Omega} \underline{\mathbf{q}}(x)\,\underline{\mathbf{q}}^{\tau}(x)\,dx\right]^{-1} \int_{\Sigma\Omega} \underline{\mathbf{q}}(x)\,\underline{\mathbf{p}}^{\tau}(x)\,dx\right\} \underline{\mathbf{w}}(t) = \underline{\hat{\mathbf{w}}}(t) \qquad [C8]$$

therefore the linear transform from $\underline{\mathbf{w}}(t)$ to $\underline{\hat{\mathbf{w}}}(t)$ can be expressed as follow:

$$\underline{\hat{\mathbf{w}}}(t) = \underline{\underline{\mathbf{H}}}\,\underline{\mathbf{w}}(t) \qquad [C9]$$

where the operator $\underline{\underline{\mathbf{H}}}$ is given by:

$$\underline{\underline{\mathbf{H}}} = \left[\int_{\Sigma\Omega} \underline{\mathbf{q}}(x)\,\underline{\mathbf{q}}^{\tau}(x)\,dx\right]^{-1} \int_{\Sigma\Omega} \underline{\mathbf{q}}(x)\,\underline{\mathbf{p}}^{\tau}(x)\,dx \qquad [C10]$$

List of Symbols

Symbol	Description	Unit
$\underline{\underline{\mathbf{0}}}_{m\times n}$	Zero-filled matrix of $m \times n$ dimension	
a	Specific surface area of electrodes	1/m
A_C	Area for the electrode/current collector interface	m^2
$a_k\ b_k$	Parameter in the solid phase diffusion equation	
Bi	Index set for non-insulation boundary nodes	
$\underline{\underline{\mathbf{B}}}_{LS}$	Operator for reference potentials	
$\underline{\underline{\mathbf{Br}}}$	Operator for reference boundary condition	
c_0	Average electrolyte concentration	mol/m^3
$\underline{\mathbf{C}}_1\ \underline{\mathbf{C}}_2$	Vectors for limiting electrical equations	
$c_L(x,t)$	Electrolyte concentration	mol/m^3
$\hat{c}_{L,i}(t)$	Element-average electrolyte concentration	mol/m^3
$\underline{\mathbf{c}}_L(t)$	Node value vector for electrolyte concentration	mol/m^3
$\underline{\hat{\mathbf{c}}}_L(t)$	Element-average vector for electrolyte concentration	mol/m^3
c_{max}	Maximum concentration in solid phase	mol/m^3
D_L^{eff}	Effective diffusivity of electrolyte	m^2/s
$D_{L,bulk}$	Diffusivity of bulk electrolyte	m^2/s
D_s	Diffusivity of solid phase	m^2/s
F	Faraday constant	C/mol
$\underline{\underline{\mathbf{F}}}$	Forcing matrix	
$\underline{\mathbf{h}}$	Operator for boundary current	
$\underline{\underline{\mathbf{H}}}$	Operator for element-average values	
$\underline{\underline{\mathbf{I}}}_{m\times m}$	Identity matrix of $m \times m$ dimension	
I_{1C}	Current for 1 C rate	A
I_{app}	Applied current	A
I_{ex}	Current at cell terminals	A
i_B	Boundary current density	A/m^2
$\underline{\underline{\mathbf{J}}}_{m\times n}$	One-filled matrix of $m \times n$ dimension	
$\underline{\underline{\mathbf{Jac}}}$	Jacobian matrix	
j_0	Reference state exchange current density	A/m^2
$j_{ex,i}$	Exchange current density	A/m^2
$j_s(x,t)$	Surface electrochemical current density	A/m^2
$\underline{\mathbf{j}}_s(t)$	Vector for surface current density	A/m^2
$\underline{\underline{\mathbf{K}}}$	Stiffness matrix	
$l_n\ l_p\ l_s$	Thickness of anode, separator, cathode	m
$\underline{\mathbf{L}}_B$	Boundary loading vector	
m	Total number of elements	
m'	Number of elements in electrode domains	
m_1	Number of elements in anode	
m_2	Number of elements in separator	
m_3	Number of elements in cathode	
$\underline{\underline{\mathbf{M}}}$	Mass matrix	
n	Total number of nodes	
n'	Number of nodes in electrode domains	
n_1	Node index for anode/separator interface	
n_2	Node index for separator/cathode interface	
n_B	Boundary outward normal vector	
P_{app}	Applied power	W
$p_i(x)\ q_i(x)$	Basis functions	
$\underline{\mathbf{p}}_{ac}(x)\ \underline{\mathbf{q}}_{ac}(x)$	Basis function vectors for anode and cathode domains	
$\underline{\mathbf{p}}_{asc}(x)\underline{\mathbf{q}}_{asc}(x)$	Basis function vectors for entire geometry	
$Q_{i,k}(t)$	Eigenfunction for solid phase diffusion	
R	Universal gas constant	J/mol/K
$\underline{\mathbf{R}}_{BV}$	Residue vector for Butler-Volmer equation	
$\underline{\mathbf{R}}_{CE}$	Residue vector for control equation	
$\underline{\mathbf{R}}_{LE}$	Residue vector for limiting electrical equation	
R_{ex}	External resistance	Ω
R_{film}	Resistance of SEI film	Ωm^2
$\underline{\underline{\mathbf{R}}}_{film}$	Matrix operator for film resistance	Ωm^2
$\underline{\mathbf{Res}}$	Residue vector	
$R_{load}(t)$	Dynamic load resistance	Ω
R_s	Radius for solid phase particles	m
t	Time	s
T	Temperature	K
t^+	Electrolyte transference number	
U	Open circuit potential	V
U^*	Modified open circuit potential	V
$\underline{\mathbf{U}}$	Vector for modified open circuit potential	V
$u_B\ z_B$	Coefficients for linear boundary current expression	
V_{app}	Applied voltage	V
$w(x,t)$	Dependent variable for the standard equation	
$\underline{\mathbf{w}}(t)$	Node value vector for dependent variable	
$\underline{\hat{\mathbf{w}}}(t)$	Element-average value vector for dependent variable	
x	Linear coordinate	m
x_i	Coordinate of node points	m
Δx_i	Length of element	m
$\underline{\mathbf{y}}$	Unknown vector for algebraic constraints	
Δy	Step change for unknown vector	
$\underline{\underline{\mathbf{Z}}}_L\ \underline{\underline{\mathbf{Z}}}_S\ \underline{\underline{\mathbf{Z}}}_k\ \underline{\underline{\mathbf{Z}}}_\Delta$	Resistance operators	Ωm^2
$\gamma(x)$	Forcing function	
ε_L	Porosity of the void phase of the electrolyte	
ε_S	Volume fraction of solid phase	
η	Electrochemical over potential	V
$\underline{\boldsymbol{\eta}}$	Vector for over potential	V
$\theta_i^*(t)$	Solid phase surface state-of-charge	

$\theta_{\text{avg},i}(t)$	Average state-of-charge in solid phase	
$\kappa_{\text{L}}^{\text{eff}}$	Effective electrical conductivity of electrolyte	
$\kappa_{\text{L,bulk}}$	Electrical conductivity of bulk electrolyte	
$\mu(x,t)$	Transport coefficient	
$\rho(x)$	Mass function	
$\sigma_{\text{S}}^{\text{eff}}$	Effective electrical conductivity of solid phase	S/m
τ	Superscript meaning transpose	
$\phi_{\text{L}}(x,t)$	Electrical potentials for electrolyte	V
$\phi_{\text{L}}^{*}(x,t)$	Modified electrical potentials for electrolyte	V
$\hat{\phi}_{\text{L},i}^{*}(t)$	Element-average value for modified electrolyte potential	V
$\phi_{\text{L}}^{\text{ref}}(t)$	Reference electrolyte potential	V
$\underline{\boldsymbol{\Phi}}_{\text{L}}(t)$	Node value vector for modified electrolyte potential	V
$\underline{\hat{\boldsymbol{\Phi}}}_{\text{L}}(t)$	Element-average vector for modified electrolyte potential	V
$\phi_{\text{S}}(x,t)$	Electrical potentials for solid phase	V
$\phi_{\text{S}}^{*}(x,t)$	Modified electrical potentials for solid phase	V
$\hat{\phi}_{\text{S},i}^{*}(t)$	Element-average value for modified solid phase potential	V
$\phi_{\text{S}}^{\text{ref}}(t)$	Reference solid phase potential	V
$\underline{\boldsymbol{\Phi}}_{\text{S}}(t)$	Node value vector for modified solid phase potential	V
$\underline{\hat{\boldsymbol{\Phi}}}_{\text{S}}(t)$	Element-average vector for modified solid phase potential	V

References

1. T. F. Fuller, M. Doyle, and J. Newman, "Simulation and Optimization of the Dual Lithium Ion Insertion Cell," *Journal of the Electrochemical Society*, **141**(1), 1 (1994).
2. S. Santhanagopalan, Q. Z. Guo, P. Ramadass, and R. E. White, "Review of models for predicting the cycling performance of lithium ion batteries," *Journal of Power Sources*, **156**(2), 620 (2006).
3. G. G. Botte, V. R. Subramanian, and R. E. White, "Mathematical modeling of secondary lithium batteries," *Electrochimica Acta*, **45**(15), 2595 (2000).
4. V. Ramadesigan, P. W. C. Northrop, S. De, S. Santhanagopalan, R. D. Braatz, and V. R. Subramanian, "Modeling and Simulation of Lithium-Ion Batteries from a Systems Engineering Perspective," *Journal of the Electrochemical Society*, **159**(3), R31 (2012).
5. P. W. C. Northrop, B. Suthar, V. Ramadesigan, S. Santhanagopalan, R. D. Braatz, and V. R. Subramanian, "Efficient Simulation and Reformulation of Lithium-Ion Battery Models for Enabling Electric Transportation," *Journal of the Electrochemical Society*, **161**(8), E3149 (2014).
6. L. Cai and R. E. White, "Reduction of Model Order Based on Proper Orthogonal Decomposition for Lithium-Ion Battery Simulations," *Journal of the Electrochemical Society*, **156**(3), A154 (2009).
7. V. Ramadesigan, V. Boovaragavan, J. C. Pirkle, and V. R. Subramanian, "Efficient reformulation of solid-phase diffusion in physics-based lithium-ion battery models," *Journal of the Electrochemical Society*, **157**(7), A854 (2010).
8. T. R. Ashwin, A. McGordon, W. D. Widanage, and P. A. Jennings, "Modified electrochemical parameter estimation of NCR18650BD battery using implicit finite volume method," *Journal of Power Sources*, **341**, 387 (2017).
9. K. A. Smith, C. D. Rahn, and C. Y. Wang, "Control oriented ID electrochemical model of lithium ion battery," *Energy Conversion and Management*, **48**(9), 2565 (2007).
10. K. A. Smith, C. D. Rahn, and C. Y. Wang, "Model-based electrochemical estimation and constraint management for pulse operation of lithium ion batteries," *IEEE Transactions on Control Systems Technology*, **18**(3), 654 (2010).
11. K. A. Smith, C. D. Rahn, and C. Y. Wang, "Model-based electrochemical estimation of lithium-ion batteries," 2008 *IEEE International Conference on Control Applications*: p. 714.
12. M. Guo and R. E. White, "A distributed thermal model for a Li-ion electrode plate pair," *Journal of Power Sources*, **221**, 334 (2013).
13. M. Guo, G. H. Kim, and R. E. White, "A three-dimensional multi-physics model for a Li-ion battery," *Journal of Power Sources*, **240**, 80 (2013).
14. M. Guo and R. E. White, "Mathematical model for a spirally-wound lithium-ion cell," *Journal of Power Sources*, **250**, 220 (2014).
15. M. Guo, X. Jin, and R. E. White, "Nonlinear State-Variable Method for Solving Physics-Based Li-Ion Cell Model with High-Frequency Inputs," *Journal of the Electrochemical Society*, **164**(11), E3001 (2017).